Iranian Polymer Journal (2022) 31:31–57
https://doi.org/10.1007/s13726-021-00982-1

REVIEW

Supercapacitor performances of titanium–polymeric nanocomposites: a review study

Murat Ates[1] · Ozge Kuzgun[1] · Idris Candan[2]

Received: 1 April 2021 / Accepted: 25 July 2021 / Published online: 18 September 2021

Abstract

This review article presents a research and technological investigation on supercapacitors and describes the recent advances of titanium-based materials in these areas. The introduction covers the properties of titanium materials, electrochemical performances of total stored charges, electric double layer capacitance (EDLC), and pseudocapacitance. The following two sections focus on the synthesis and capacitance results of titanium carbide (Ti_3C_2Tx) and titanium nitride (TiN), respectively. In the last section of this review, the role of titanium dioxide (TiO_2) is demonstrated in the supercapacitors of TiO_2-based, carbon/TiO_2-based, metal/TiO_2-based, and conducting polymer/TiO_2 nanocomposites. Many factors affect the electrochemical performance of supercapacitor devices, such as doping process, conductivity, interaction between components of nanocomposite, electrolyte type, and structure type, etc. In the end, future perspectives and challenges are summarized and considered for future TiO_2-based nanocomposite supercapacitors. A total of 182 references are cited to understand the effects of TiO_2-based materials on supercapacitor device performances.

Graphic abstract

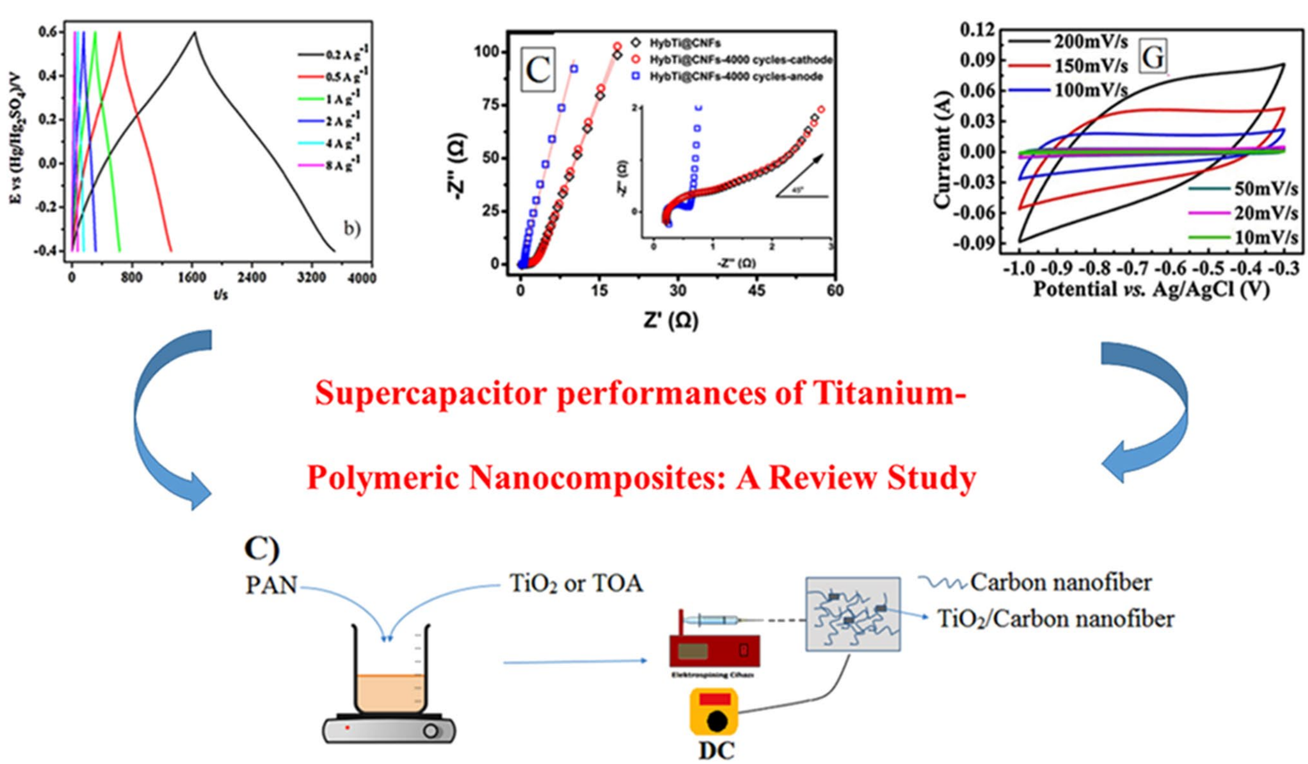

Keywords Titanium carbide · Titanium nitride · Titanium dioxide · Supercapacitor · EDLC

Abbreviations

AC	Alternative current
Ti_3C_2Tx/Al	Aluminum interlayers
PM4EOT	Alkoxy-functionalized polythiophene
CNT	Carbon nanotube
CNFs	Carbon nanofibers
C	Carbon
CC	Carbon cloth
CL	Chrysanthemum-like
CoS	Cobalt (II) sulfur
$CoMoO_4$	Cobalt molybdate
CV	Cyclic voltammetry
CMC	Carboxymethyl cellulose
EDLC	Electric double layer capacitance
EIS	Electrical impedance spectroscopy
GCD	Galvanostatic charge–discharge
GCE	Glassy carbon electrode
GN	Graphene
GO	Graphene oxide
ΔG	Gibbs-free energy
LiCl	Lithium chloride
Li_2SO_4	Lithium sulfate
MnO_2	Manganese (IV) oxide
MoO_3	Molybdenum trioxide
MoS_2	Molybdenum disulfide
$Ti_3C_2T_x/\alpha\text{-}Fe_2O_3$	MXene materials
MWCNT	Multiwalled carbon nanotube
NG	*N*-Doping graphene
NPs	Nanoparticles
NWA	Nanowire
Ni	Nickel
Ni-MOF	Nickel metal–organic framework
1D	One-dimensional
R_s	Ohm resistance
3D $Ti_3C_2T_x$ aerogel	Paper electrode
H_3PO_4	Phosphoric acid
PEDOT	Poly(3,4-ethylenedioxythiophene)
PANI	Polyaniline
$PANI/TiO_2/Ti_3C_2T_x$	Polyaniline nanoflakes and TiO_2 nanoparticles
PPy	Polypyrrole
KOH	Potassium hydroxide
KCl	Potassium chloride
PTh	Polythiophene
PEDOT	Poly(3,4-ethylenedioxythiophene)
rGO	Reduced graphene oxide
RuO_2	Ruthenium (IV) oxide
Na_2SO_4	Sodium sulfate
(SWCNT)	Single-walled carbon nanotube
C_s or C_{sp}	Specific capacitance
(SCs)	Supercapacitors
S	Sulfur
H_2SO_4	Sulfuric acid
Ti	Titanium
TiN	Titanium nitride
$TiN/NiCo_2O_4$	Titanium nitride nanoarray
$Ti_3C_2T_x$ or Ti_3C_2	Titanium carbide
TiO_2	Titanium dioxide
MXene	Transition metal carbides, nitrides or carbonitrides
MnO_x/Ti_3C_2	Titanium carbide nanosheets and manganese oxide nanoparticles
VO_5	Vanadium penta oxide
VN	Vanadium nitride
WO_3	Tungsten trioxide
$\alpha\text{-}MoO_3$-nanoplate	α-Molydenum oxide nanoplate

Introduction

Supercapacitors are considered to play an important role in power devices and energy storage systems in future generations [1–3]. Owing to the fast storage (as high as 100 thousand times) and large power (~ 10 kW/kg) and energy capacities, supercapacitors make a great enhancement in advanced energy applications [4–6]. Recently, supercapacitors have been expanded on structural architecture, material production, performance analysis, and understanding of the significant electrochemical phenomena. Efficient energy storage systems and clean environmental energy sources are crucial issues for the contemporary society due to the rapid developments made in the technology and industry in today energy-dependent world. Supercapacitors [7–9], batteries [10, 11] and fuel cells [12, 13] can be used to solve these issues. One of the most important energy storage systems is supercapacitors (SCs), which have attracted more interest than batteries, because they have fast charged/discharged capability and long cyclic stability as emerging energy storage devices [14–16]. Supercapacitors are used in many hybrid electroactive materials which have carbon-based materials and metal oxides with reversible redox reactions [17, 18]. Supercapacitors are divided into three main parts depending on the charge storage capability: EDLC [19], pseudocapacitor [20], and hybrid supercapacitors [21–25]. Supercapacitors have a combination of fundamental features for energy storage systems [26, 27]. These are energy and power density [28], good stability, fast charge/discharge capability, etc. [29–31]. Hybrid supercapacitors are used to improve device performances based on the carbon materials in EDLC system and pseudocapacitive materials, such as metal oxides [32, 33] or conducting polymers [34–36]. In this review article, we chose the titanium-based supercapacitors supplying faradaic effects and combining with other materials providing high thermal stability, chemical stability, low cost, and low toxicity [37–39].

Historical overview of supercapacitors

The development of capacitors started on the storage of electrical charges using a metal and an electrolytic solution in the nineteenth century [40]. General Electric Co. presented a patent for porous carbon electrode in 1957 [41, 42]. Evans explained the terms of faradaic charge transfer between electrodes and ions [43]. It was partly explained by Helmoltz plane and faradaic reactions in the anode and cathode compartments. Nowdays, numerous electroactive materials can be prepared to perform EDLC, pseudocapacitors, and hybrid supercapacitor systems. Synthesis of hybrid systems can be useful to improve electrochemical performance of supercapacitors [44, 45].

Titanium-based nanocomposites

Transition metal carbide materials, such as titanium carbide ($Ti_3C_2T_x$)-based materials have the following characteristic properties: high melting point (up to 3260 °C), remarkable chemical and thermal stability, high rigidity, and high electrical conductivity [46–48]. Ti_2CT_x are the lightest transition metal carbides, nitrides, or carbonitrides (MXene) and supposed to have a larger surface capacity than $Ti_3C_2T_x$ for the larger surface area and more functional groups per unit mass [49, 50]. Titanium carbide is synthesized by replacement of titanium (Ti) or TiO_2 and carbon (C) element at high temperatures between 1500 and 2300 K. The reaction temperature should be taken at higher temperatures as compared to other carbides. Moreover, the higher temperature supplies quick reaction and diffusion of carbon material into the metal or metal oxides.

Titanium nitride (TiN) is another material that has many advantages, such as high melting point, good mechanical stability, low cost, and high electrical conductivity [51, 52]. Thus, supercapacitors have fast charge movements and charge accumulation. TiN is used for electrochemical energy storage devices, coating technology, sensors technology, and battery technology [53, 54].

Titanium dioxide (TiO_2) is used as an electroactive materials for supercapacitors. It has more advantageous than other metal oxides, such as ruthenium (IV) oxide (RuO_2), vanadium (V) oxide (VO_5), molybdenum trioxide (MoO_3), and cobalt (II) sulfur (CoS) due to low cost, environmentally friendly, and high chemical stability [55–58]. TiO_2 has different names, such as TiO_2 (B), brookite, anatase, and rutile [59–61]. Additional research studies are needed to develop the surface morphology, doping process, and energy-power density [62, 63]. However, TiO_2-based supercapacitors have still low electrochemical performances [64]. Therefore, we need to improve the electrochemical performances of supercapacitors with respect to their low cost and highly efficient properties. Sandwich composite of amorphous titanium dioxide/polyaniline/graphene oxide (TiO_2/PANI/GO) was used as an anode material for lithium-ion batteries (LIBs). A first discharge capacity was used as 1335 $mAhg^{-1}$ at 50 mAg^{-1} [65]. The amorphous states of many intercalation metal oxides, such as TiO_2 have better power density than crystalline forms [66].

EDLC, pseudocapacitance, and hybrid supercapacitors

In a typical supercapacitor, the charge becomes stored either by total charges in EDLC or pseudocapacitors with redox reactions [67–69]. The basic mechanism of EDLC corresponds to a typical capacitance mechanism of dielectric capacitor, since there is no ionic or electronic transfer causing a chemical reaction (non-Faradaic charge transfer) [70–72]. In EDLC system, charges can be stored electrostatically due to reversible reactions [73]. Each material used in supercapacitor affects the performance of the device. The choice of electrode material is important to decide good electrochemical performance of device. The double layer in the interface can be created quickly, so high power density is a natural characteristic of EDLC as compared to a conventional battery where mass transport is required over longer distances [74, 75]. EDLC mechanism is caused by surface process of the electrode. So, it produces an important effect on the capacitance values. Carbon materials, such as nanotubes [76], fibers [77], graphene [78], and foams [79] are used in EDLC system due to their high surface area, low cost, etc. [80]. Furthermore, carbon materials are mainly combined with metal oxides and conducting polymers to fabricate nanocomposite electrodes [81]. One-dimensional (1D) nanostructured composites, including carbon materials and metal oxides have been mostly used in batteries and supercapacitors [82, 83]. The reason for the redox reactions is that their Gibbs-free energy (ΔG) is negative [84]. Low electrical conductivity affects the limited charge/discharge stability. The capacitance value of pseudocapacitor is 10–100 times greater than that of EDLC [85]. The pseudocapacitance behavior shows a consequence of reversible redox reactions [86–88].

The other configuration of capacitor is the hybrid supercapacitors, which enhances the energy density of supercapacitor device to a range of 20–30 Wh kg^{-1} [89]. The principles of hybrid supercapacitors are the combination of the EDLC and pseudocapacitors [90]. The better design of supercapacitor device supplies on the enhancement of energy density criteria in EDLC in order to use better electrode and electrolyte materials. The hybrid supercapacitor formation comes from coupling of different redox reactions (faradaic charge transfer) and EDLC materials like graphene (theoretical specific area, 2630 cm^2g^{-1}) [91–93] or graphite [94], metal oxides [95], conducting polymers [96], and activated carbon, etc. [97, 98]. The limiting property of EDLC is not present in the pseudocapacitor, their combination together leads to showing of the limitations of the combining components, with an advantage of presenting higher capacitance values. As a result, the hybrid supercapacitors are capable of storing a large amount of charge provided at high power rates compared to rechargeable batteries [99–101].

Titanium carbide ($Ti_3C_2T_x$)

Synthesis of $Ti_3C_2T_x$

MXenes are 2D transition metal carbides or nitrides which were discovered in 2011 [102]. These are used in energy storage systems, such as supercapacitors, batteries, and electro-catalysis. The synthetic illustrations of titanium carbide (Ti_3C_2) [103], a paper electrode (3D $Ti_3C_2T_x$ aerogel) which is subsequently prepared through vacuum-assisted filtration of the $Ti_3C_2T_x$ nanosheet suspension [104], Ti_3AlC_2 which is partially removed by simple hydrothermal etching to obtain $Ti_3C_2T_x$ reserving appropriate Al interlayers ($Ti_3C_2T_x$/Al) [105], MXene materials ($Ti_3C_2T_x$/α-Fe_2O_3) [106], mono and hexahybrid forms that are synthesized hydrothermally in one step by meticulously controlling the WO_3 (2D Ti_3C_2/WO_3) phase [107], few layered titanium carbide nanosheets and manganese oxide nanoparticles (MnO_x/Ti_3C_2) [108] and PANI nanoflakes and TiO_2 nanoparticles (PANI/TiO_2/$Ti_3C_2T_x$) [109] nanocomposites are presented in Fig. 1. There are many synthesis procedures for Ti_3C_2 and $T_3C_2T_x$ nanocomposites. These methods are chemical method, hydrothermal process, vacuum-assisted filtration, heat treatment, and in situ polymerization techniques.

Capacitance results of a paper electrode ($Ti_3C_2T_x$)

Cyclic voltammogram (CV) measurements were obtained in 1 M lithium sulfate (Li_2SO_4) solution for Ti_3C_2 material over the voltage range between − 0.9 and − 0.3 V, at a scan rate of 2–1000 mV/s as given in Fig. 2a. The CV plots still show a relatively rectangular box shape even at the higher scan rates up to 1000 mV/s. Therefore, it has a low contact resistance and a high rate capability. There are no redox peaks in the CV plots during charge/discharge processes. The specific capacitance was obtained as $C_{sp}=370$ Fg^{-1} at the scan rate of 2 mVs^{-1} for the binder-free Ti_3C_2 foam electrodes. $Ti_3C_2T_x$ aerogel was performed by CV method in the voltage range from − 0.6 to 0.2 V at a scan rate of 50 to 2000 mVs^{-1} in 3 M sulfuric acid (H_2SO_4) solution as shown in Fig. 2b. The shapes of CV curves are acceptable for supercapacitor device to work. The aerogel electrode has reached the highest capacitance of $C_{sp}=438$ Fg^{-1} at 10 mVs^{-1}. $Ti_3C_2T_x$/Al electrode was used by CV method in 0.5 M Na_2SO_4 at various scan rates in the voltage range between 0 and 0.9 V. Figure 2c shows CV plots of $Ti_3C_2T_x$/Al electrode. As seen from the figure, the device with $Ti_3C_2T_x$/Al electrode shows a good performance with a high areal capacitance of $C_{sp}=242.3$ $mFcm^{-2}$ at 1 mVs^{-1}. CV measurements of $Ti_3C_2T_x$/α-Fe_2O_3 electrode were made in 5 M lithium chloride (LiCI) solution at the voltage range of − 1.2 to 0 V. The CV curves of the $Ti_3C_2T_x$/α-Fe_2O_3 electrodes in 5 M LiCI solution as a function of the voltage range of − 1.2 to 0 V at different scan rates from 5 to 200 mVs^{-1} are presented in Fig. 2d. Two pairs of redox peaks are obvious at different scan rates as seen clearly from Fig. 2d, even at high scan rates, such as 200 mVs^{-1}. The CV results imply that the $Ti_3C_2T_x$/α-Fe_2O_3 possesses a high rate performance. A 0.5 M H_2SO_4 was used as the electrolyte for Ti_3C_2/WO_3 and potential window of − 0.5 to 0 V. Figure 2e shows the CV curves of 2D Ti_3C_2/WO_3 at scan rates varying from 2 to 100 mVs^{-1}. Apparently, the absence of redox peaks in CV curves with symmetric rectangular shape indicates fast and reversible reaction kinetics. The increase in the current density with the scan rate highlights appreciable ionic charge transport even at higher scan rates, suggesting the excellent rate capability of electrodes. The MnO_2/$Ti_3C_2T_x$ nanocomposite was used in 1 M sodium sulfate (Na_2SO_4) electrolyte solution to perform the CV measurement by the potential range of 0–0.8 V. As demonstrated in Fig. 2f, the CV curves of the flexible supercapacitor can still keep the rectangular shapes even at higher scan rates, such as 250 mVs^{-1}. Cyclic voltammograms (CVs) of MnO_x–Ti_3C_2 films were obtained in the voltage range between − 1 and − 0.3 V with scan rates of 2–200 mVs^{-1} in 1 M Li_2SO_4 solution. MnO_x–Ti_3C_2 nanocomposites have good CV profiles even up to 200 mVs^{-1} as given in Fig. 2g. Therefore, it has outstanding reversibility and high scan rate capability. This electrode has a volumetric capacitance as high as $C_{sp}=392.9$ Fcm^{-3} at 2 mVs^{-1}. CV plots of PANI/TiO_2/$Ti_3C_2T_x$ electrode as a function of the potential range of − 0.3 to − 1 V (versus Ag/AgCl) were applied using a three-electrode system in 1 M KOH aqueous solution at various scan rates from 10 to 200 mVs^{-1}. The PANI/TiO_2/$Ti_3C_2T_x$ ternary composite shows high specific capacitance of $C_{sp}=188.3$ Fg^{-1} at 10 mVs^{-1} as clearly seen from Fig. 2h.

The galvanostatic charge/discharge (GCD) plots of Ti_3C_2 electrode are presented in Fig. 3a for various current densities from 2 to 30 Ag^{-1}. As seen from the figure [110], Ti_3C_2 material has good fast charge/discharge capability and rate

Fig. 1 Schematic illustration of the synthesis procedure of **a** Ti_3C_2 [103], **b** 3D $Ti_3C_2T_x$ aerogel [104], **c** $Ti_3C_2T_x$/Al [105], **d** $Ti_3C_2T_x$/α-Fe_2O_3 [106], **e** 2D Ti_3C_2/WO_3 [107], **f** MnO_x/Ti_3C_2 [108], and **g** PANI/TiO_2/$Ti_3C_2T_x$ nanocomposites [109]. Reprinted with permission from Refs. [103–109]. Copyright: Elsevier (Ref. [103]), Royal Society Chemistry (Ref. [104]), Wiley (Ref. [105]), Elsevier (Ref. [106]), Wiley (Ref. [107]), Elsevier (Ref. [108]), Elsevier (Ref. [109])

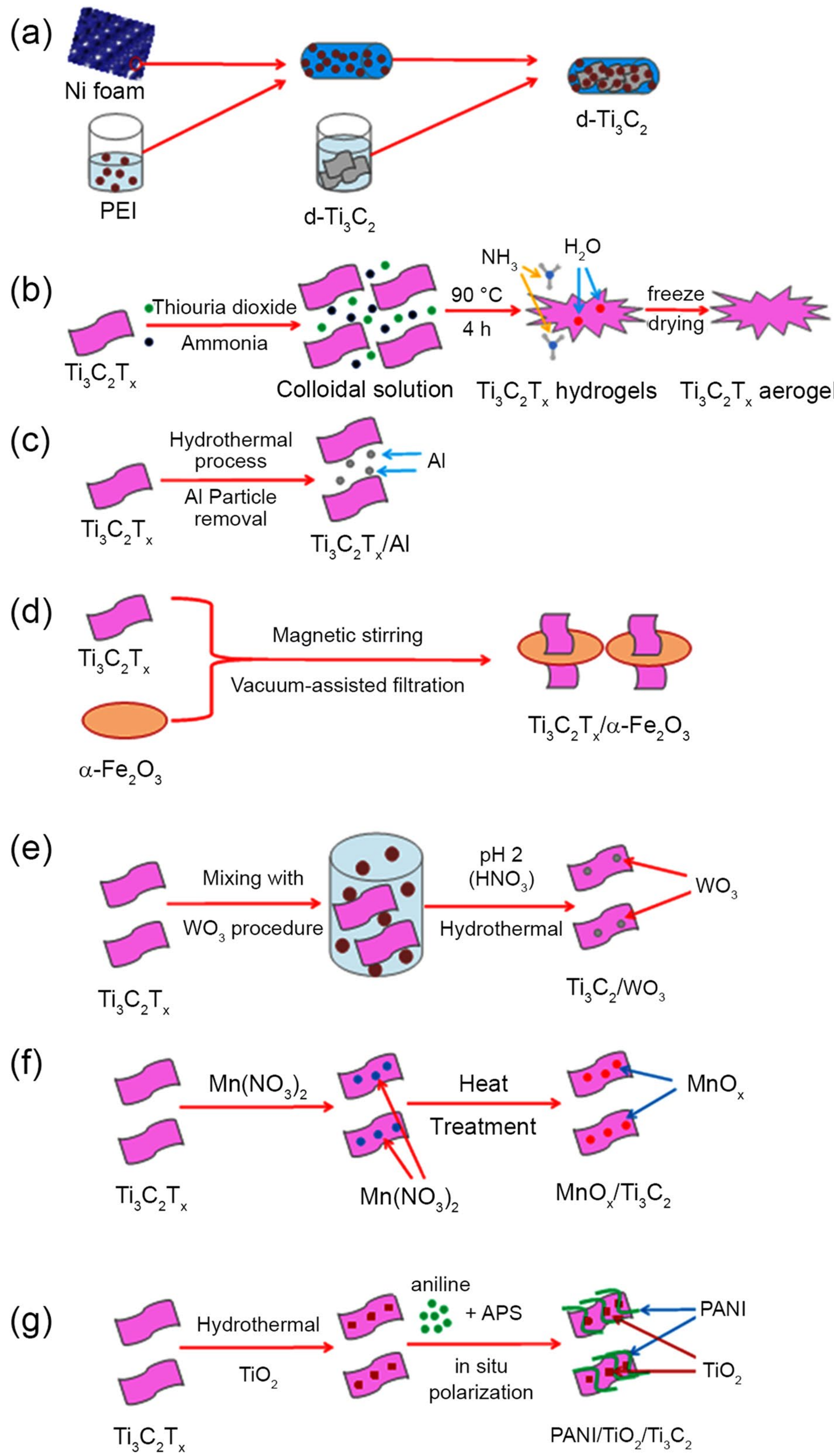

capacity at 30 Ag^{-1}. GCD measurements of $Ti_3C_2T_x$ aerogel electrode were carried out at different current densities ranging from 1 to 20 Ag^{-1}, that are given in Fig. 3b. GCD measurement results show symmetric triangular shape in the ultrahigh coulombic efficiency (~100%). On the other hand, there is no voltage drop in GCD method for $T_3C_2T_x$/Al

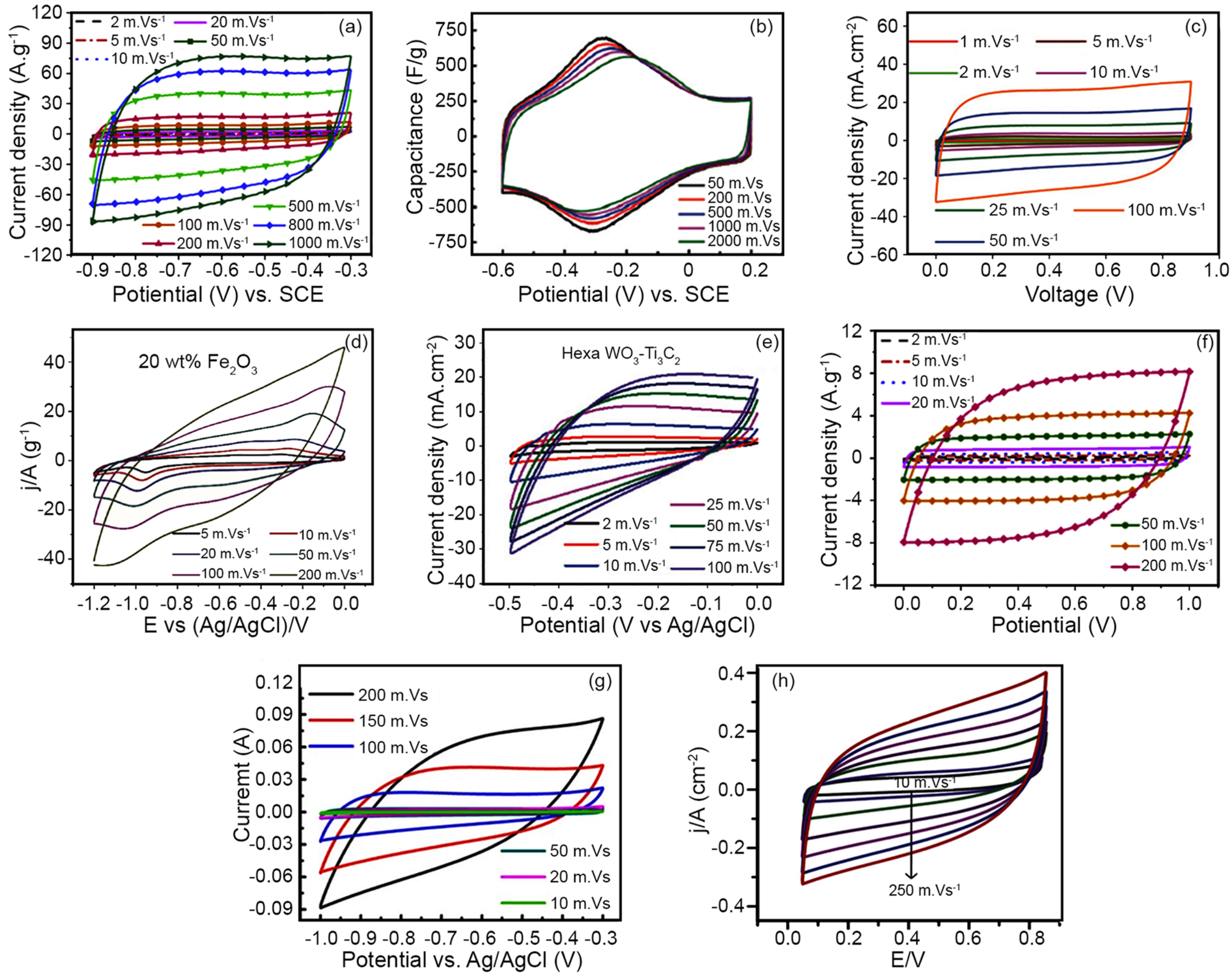

Fig. 2 CV curves of **a** T_3C_2 [103], **b** 3D $Ti_3C_2T_x$ aerogel [104], **c** $Ti_3C_2T_x$/Al [105], **d** $Ti_3C_2T_x$/α-Fe_2O_3 [106], **e** 2D Ti_3C_2/WO_3 [107], **f** MnO_x/Ti_3C_2 [108], **g** PANI/TiO_2/$Ti_3C_2T_x$ [109], and **h** MnO_2/$Ti_3C_2T_x$ [110] supercapacitors. Reprinted with permission from Refs. [103–110]. Copyright: Elsevier (Ref. [103]), Royal Society Chemistry (Ref. [104]), Wiley (Ref. [105]), Elsevier (Ref. [106]), Wiley (Ref. [107]), Elsevier (Ref. [108]), Elsevier (Ref. [109]), Elsevier (Ref. [110])

electrode as seen from Fig. 3c. The highest specific capacitance was obtained as $C_{sp} = 1087$ mFcm^{-2} at 1 mAcm^{-2}. GCD plots of the $Ti_3C_2T_x$/α-Fe_2O_3 electrodes were used at different current densities in the range of − 1.2 to 0 V. Figure 3d shows that $Ti_3C_2T_x$/α-Fe_2O_3 electrodes show both characteristics of pseudocapacitance and electric double layer capacitance (EDLC) behavior. There are a few peaks at around charge point of − 0.28 V and discharge point of − 0.95 V in the CV curves. These results are consistent with the two pairs of redox peaks displayed on the CV curves. Figure 3e presents the GCD curves of the hybrid electrode of Ti_3C_2/WO_3. As seen from Figs. 2e and 3e, these measurements are compatible with the results of CV measurements. Furthermore, the highest specific capacitance was calculated as $C_{sp} = 566$ Fg^{-1} for Ti_3C_2/WO_3 nanocomposite. The electrode of MnO_x–Ti_3C_2 film was used to obtain the GCD curves for different current densities as presented in Fig. 3f. As seen from the figure, the low internal resistance was also obtained for the MnO_x–Ti_3C_2 film using the three-electrode system. The variation of GCD curves for PANI/TiO_2/$Ti_3C_2T_x$ ternary composite is demonstrated in Fig. 3g. All the GCD curves of PANI/TiO_2/$Ti_3C_2T_x$ electrode show equilateral triangle shapes, indicating high reversibility of PANI/TiO_2/$Ti_3C_2T_x$ ternary composite during charge/discharge process. The PANI/TiO_2/$Ti_3C_2T_x$ ternary composite exhibits specific capacitance of $C_{sp} = 108.9$ Fg^{-1} at 0.5 Ag^{-1}.

Electrochemical impedance spectroscopy (EIS) is an important method to find out the electrochemical performance and understanding on the kinetics of the supercapacitor electrodes. The Nyquist plots corresponding to EIS are shown in Fig. 4a–g. All the electrodes showed a sloping line, indicating good capacitive behavior of the samples

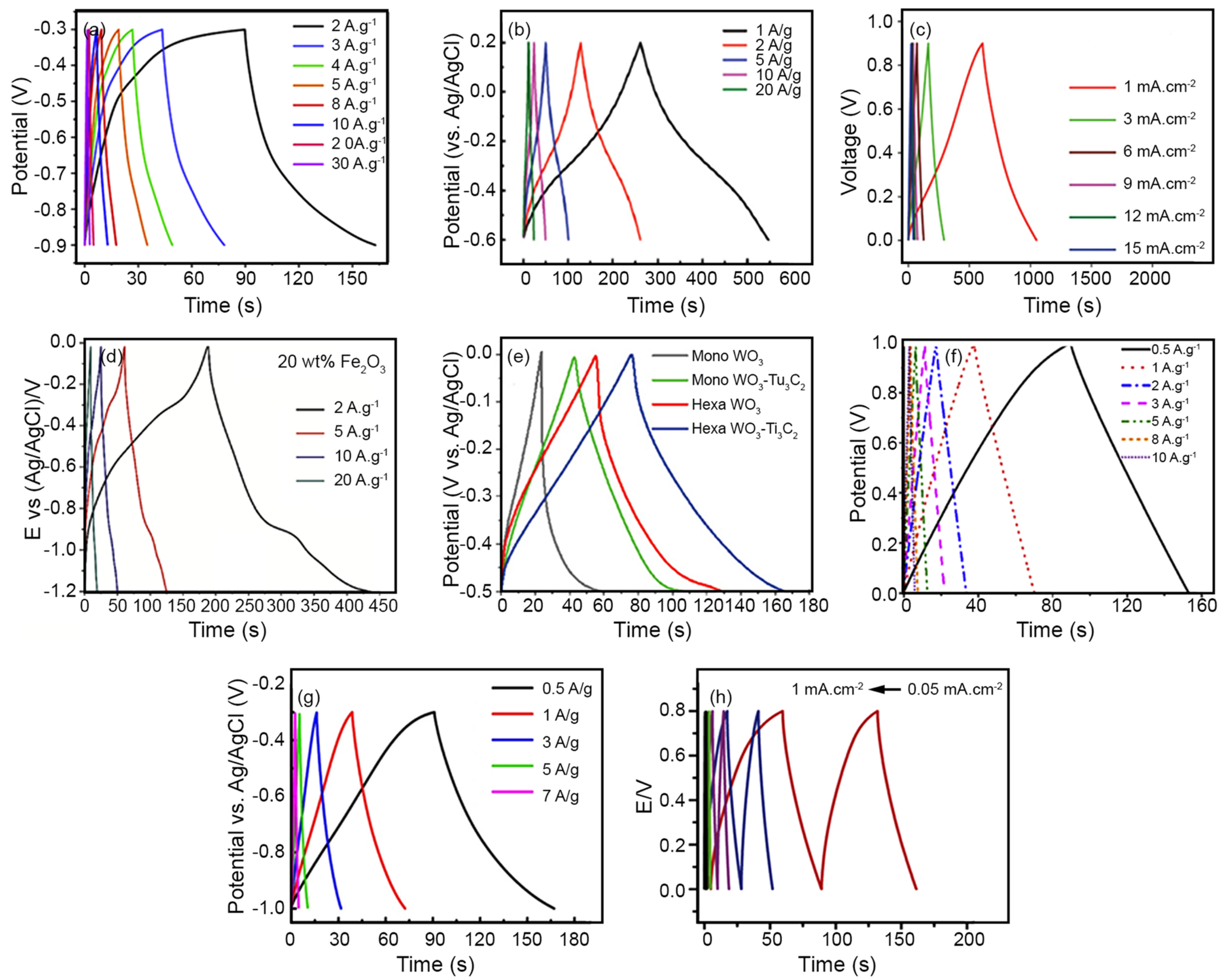

Fig. 3 Galvanostatic charge/discharge (GCD) graphs of **a** T_3C_2 [103], **b** 3D $Ti_3C_2T_x$ aerogel [104], **c** $Ti_3C_2T_x$/Al [105], **d** $Ti_3C_2T_x$/α-Fe_2O_3 [106], **e** 2D Ti_3C_2/WO_3 [107], **f** MnO_x/Ti_3C_2 [108], **g** PANI/TiO_2/$Ti_3C_2T_x$ [109] and **h** $MnO_2/Ti_3C_2T_x$ [110]. Reprinted with permission from Refs. [103–110]. Copyright: Elsevier (Ref. [103]), Royal Society Chemistry (Ref. [104]), Wiley (Ref. [105]), Elsevier (Ref. [106]), Wiley (Ref. [107]), Elsevier (Ref. [108]), Elsevier (Ref. [109]), Elsevier (Ref. [110])

at low frequency region. The ohm resistances (R_s, determined by the intersection of the real axis and the imaginary axis) corresponded the solution and internal resistances of all electrode materials at a high frequency region. These results indicate that the $Ti_3C_2T_x$ nanosheets could effectively improve conductivity, and thus significantly enhance the capacitance of all the $Ti_3C_2T_x$ electrode materials.

In litereature, there are many $Ti_3C_2T_x$ nanocomposites in various electrolytes and higher specific capacitance values as given in Table 1. Specific capacitance values can be affected by many factors, such as material structure, electrolyte type and synthesis procedure, etc. In literature, there are many papers based on the $Ti_3C_2T_x$ electrode materials [118, 119]. For instance, nickel–organic framework (Ni-MOF)/$Ti_3C_2T_x$ hybrid nanocomposite is used in supercapacitor evaluations. It shows high specific capacitance of $C_{sp} = 867.3$ Fg^{-1} at 1 Ag^{-1}. S-Ti_3C_2Tx/N–C-700 °C electrode was designed at a three-electrode system [120]. Its specific capacitance was obtained as $C_{sp} = 260$ Fg^{-1} at 0.8 Ag^{-1}, about 3 times higher than that of many other $Ti_3C_2T_x$-based materials reported in literature. Nam et al. [121] have synthesized a $Ti_3C_2T_x$ MXene material for wearable energy devices, such as supercapacitors and triboelectric nanogenerators. $Ti_3C_2T_x$ free-standing film annealed under 200 °C showed a high capacitance of $C_{sp} = 429$ Fg^{-1} and energy density of $E = 29.2$ $Whkg^{-1}$ in 1 M H_2SO_4 solution [122]. $Ti_3C_2T_x$ MXene coated metal mesh electrodes were used for stretchable supercapacitors, which showed an aneal capacitance of $C_{sp} = 33.3$ $mFcm^{-2}$ at 10 mVs^{-1} [123].

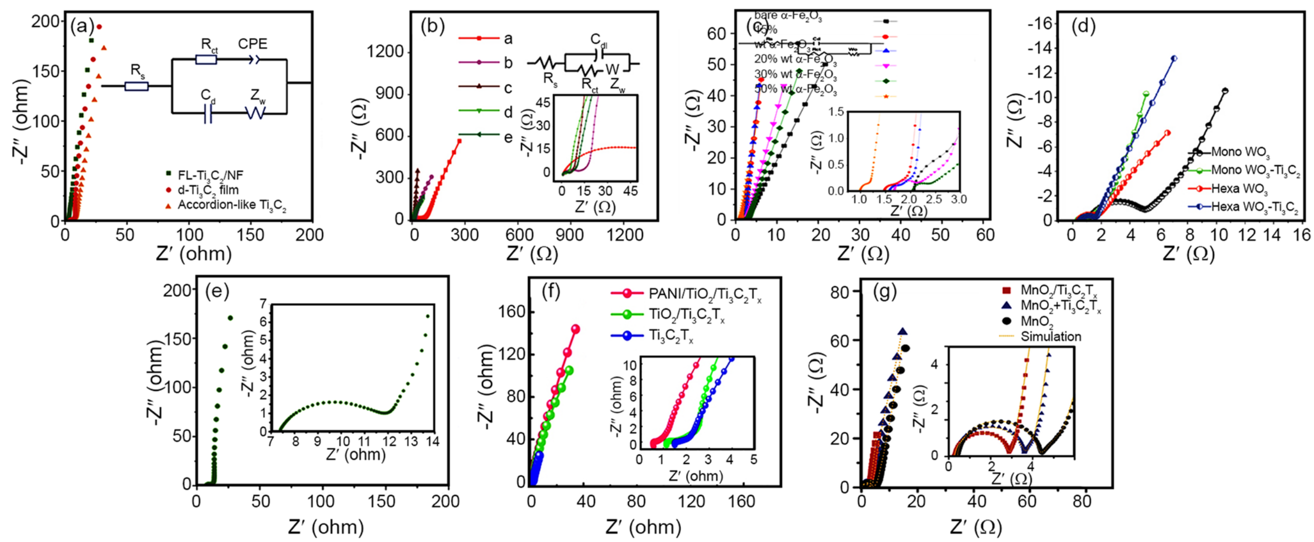

Fig. 4 Nyquist plots of **a** T_3C_2 [103], **b** $Ti_3C_2T_x$/Al [104], **c** $Ti_3C_2T_x$/α-Fe_2O_3 [105], **d** 2D Ti_3C_2/WO_3 [106], **e** MnO_2/$Ti_3C_2T_x$ [107], **f** MnO_x/Ti_3C_2 [108], and **g** PANI@TiO_2/$Ti_3C_2T_x$ [109] supercapacitor. Reprinted with permission from Refs. [103–109]. Copyright: Elsevier (Ref. [103]), Wiley (Ref. [104]), Elsevier (Ref. [105]), Wiley (Ref. [106]), Elsevier (Ref. [107]), Elsevier (Ref. [108]), Elsevier (Ref. [109])

Table 1 Capacitance results of $Ti_3C_2T_x$-based materials

Materials	Electrolyte	Capacitance	References
$Ti_3C_2T_x$ MWCNT sandwich	1 M $MgSO_4$	120 Fg^{-1} at 200 mVs^{-1}	[111]
400-KOH–Ti_3C_2	1 M H_2SO_4	200 Fg^{-1} at 100 mVs^{-1}	[112]
N-$Ti_3C_2T_x$	1 M Li_2SO_4	415.0 Fg^{-1} at 2 mVs^{-1}	[113]
TiO_2–Ti_3C_2	6 M KOH	120 Fg^{-1} at 100 mVs^{-1}	[114]
$Ti_3C_2T_x$ "clay"	1 M H_2SO_4	245 Fg^{-1} at 2 mVs^{-1}	[115]
$Ti_3C_2T_x$/PPy	1 M H_2SO_4	416 Fg^{-1} at 5 mVs^{-1}	[116]
$Ti_3C_2T_x$/ZnO	1 M KOH	120 Fg^{-1} at 2 mVs^{-1}	[117]

The other $Ti_3C_2T_x$ suspension and carbonizing the composite fabric presented the highest areal capacitance of $C_{sp}=794.2$ $mFcm^{-2}$ (233.6 Fg^{-1}) at 2 mVs^{-1} with 6% by weight $Ti_3C_2T_x$ at 1000 °C [124].

Titanium nitride (TiN)

Synthesis of TiN

The schematic synthesis procedure diagrams of chrysanthenum-like titanium nitride (CL-TİN) [125], titanium nitride nanowire array (TİN/$NiCo_2O_4$) [126], polypyrrole/titanium nitride/polyaniline coaxial nanotube hybrid (PPy/TİN/PANI) [127], and polyaniline/carbon/titanium nitride nanowire array (PANI/C/TİN NWA) [128] are presented in Fig. 5. In these synthesis processes, there are many methods used, such as heating, nitradation at high temperatures, electrodeposition process, etc.

Capacitance results of TiN

The typical CV curves of the CL-TiN/glassy carbon electrode (GCE) were obtained at different scan rates from 0.1 to 1.0 Vs^{-1}. Similar rectangular shapes are obtained even at a scan rate of 1.0 Vs^{-1} in 1 M Na_2SO_4 solution. Hence, CV plots demonstrate good capacitive behavior and show a typical characteristic of the electrical double-layer capacitor. The CV measurements of TiN NWA/$NiCo_2O_4$ electrode were carried out at various scan rates from 10 to 200 mVs^{-1} by a three-electrode system in 2 M potassium hyyroxide (KOH) solution. As seen from Fig. 6b, a pair of well-defined redox peaks can be clearly observed from all the CV curves, which refers to reversible faradaic reactions. The typical CV curves of PPy/TiN/PANI nanotube hybrid material were measured in 1.0 M H_2SO_4 solution at different scan rates from 5 to 100 mVs^{-1} (Fig. 6c). The PPy/TiN/PANI nanotube hybrid shows typical pseudocapacitor behavior because the intensity of couple peaks is directly proportional to the scan rate. As the scan rate increased, the oxidation peak shifted

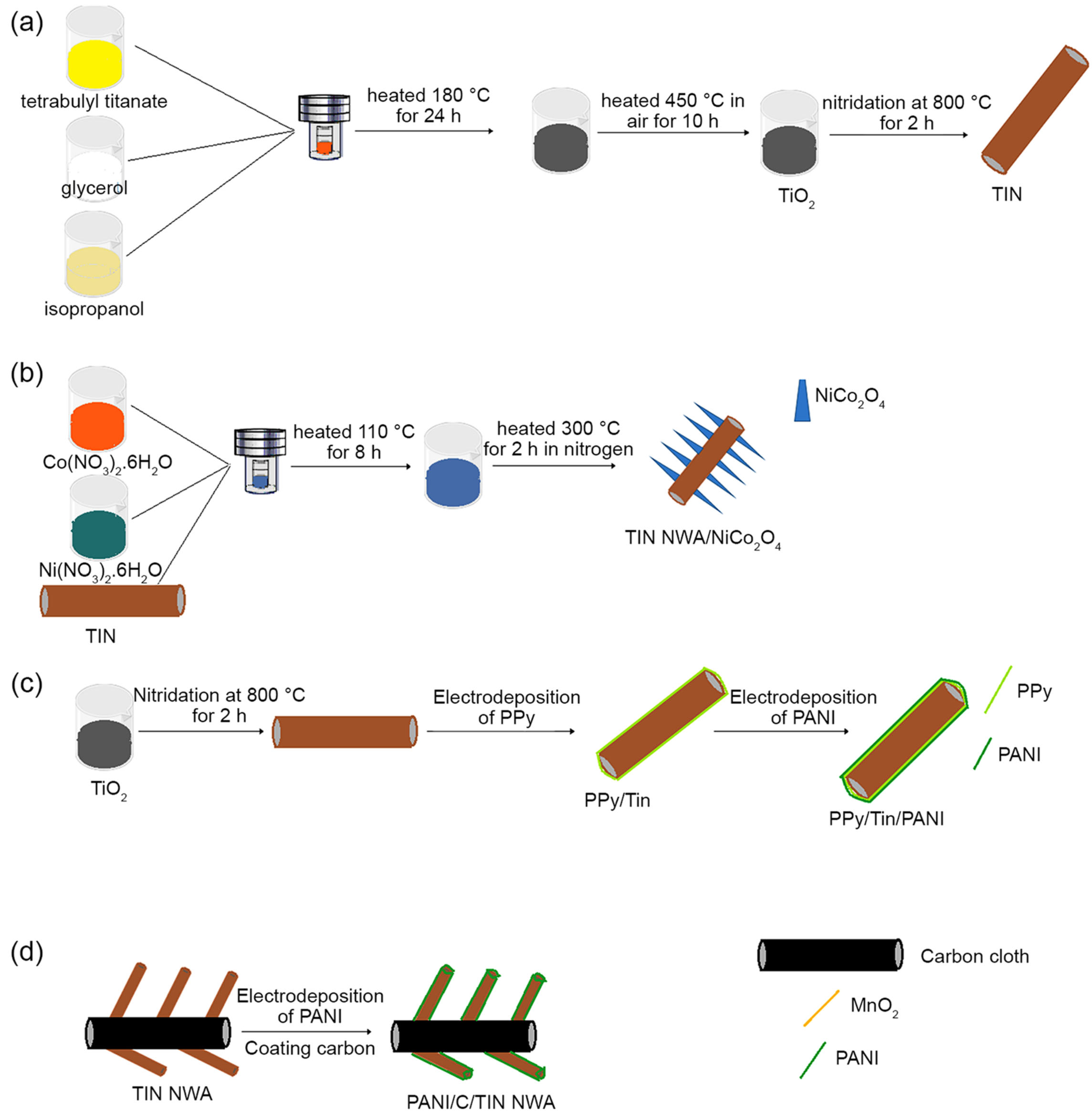

Fig. 5 Synthesis procedure of **a** CL-TiN [125], **b** TiN/$NiCo_2O_4$ [126], **c** PPy/TiN/PANI [127], and **d** PANI/C/TiN NWA [128]. Reprinted with permission from Refs. [125–128]. Copyright: Elsevier (Refs. [125–128])

to a positive value and reduction peak shifted to a negative value, accordingly.

The electrochemical performance of the supercapacitor device with CL-TİN electrode was carried out by the galvanostatic charge–discharge (GCD) measurements, which were performed at different current densities from 0.1 to 1 Ag^{-1} (Fig. 7a). The GCD curves of CL-TİN electrode are nearly linear and symmetric triangles, showing a good capacitance performance of the device. The specific capacitance of $C_{sp}=23.35$ Fg^{-1} was computed for the CL-TiN electrode at current density of 1.0 Ag^{-1} using a three-electrode system. Furthermore, the cycle life is one of the most important parameters to measure the stability of the supercapacitor electrode materials. Even after 20,000 cycles at a scan rate of 10 Vs^{-1}, the specific capacitance of CL-TiN endured at 89.8% of the initial specific capacitance. The GCD measurements of the TiN NWA/$NiCo_2O_4$ nanocomposite with increasing discharge current density (5, 10, 20, 50, and 100 Ag^{-1}) are given in literature [98]. All the potential–time curves at different current densities are almost symmetric, showing a good electrochemical capacitance performance of the TiN NWA/Ni-Co_2O_4 nanocomposite. In addition, these charge/discharge voltage plateaus match the well-defined redox peaks observed in the CV curves. The specific capacitance of the TiN NWA/$NiCo_2O_4$ composite on carbon cloth (CC) electrode was obtained as $C_{sp}=1200$ Fg^{-1} at current

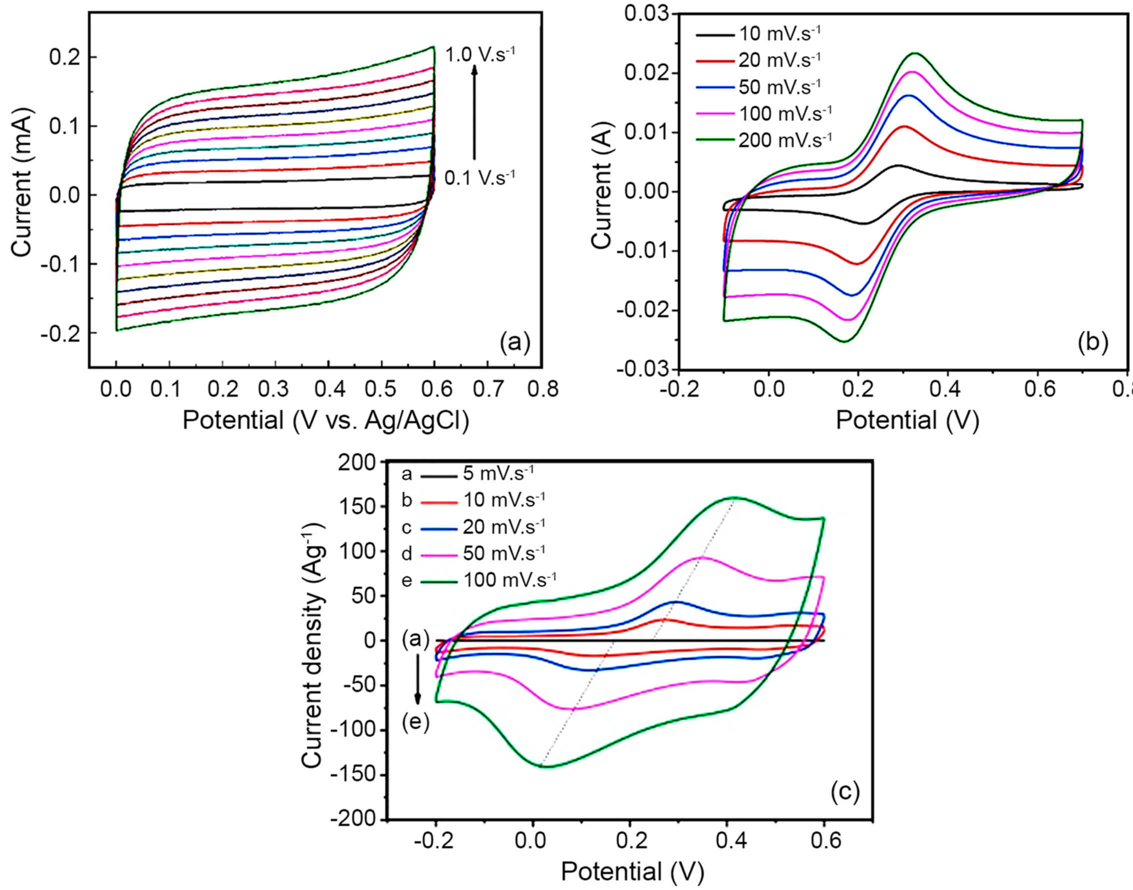

Fig. 6 CV curves of **a** CL-TiN [125], **b** TiN/$NiCo_2O_4$ [126] **c** PPy/TiN/PANI [127], and **d** PANI/C/TiN NWA [128]. Reprinted with permission from Refs. [125–128]. Copyright: Elsevier (Refs. [125–128])

density of 2.0 Ag^{-1}. There are many factors that affect GCD method, such as mass of active materials, potential window, discharge time, and discharge current, etc. [129]. The GCD curves and capacitance curve of PPy/TiN/PANI nanotube hybrid material were studied at different current densities from 0.5 to 20 Ag^{-1} (Fig. 7b). The capacitance value was found inversely proportional to current density. The capacitance gradually decreased with increasing current density and then gradually achieved a relatively stable level. The corresponding specific capacitance was obtained as $C_{sp} = 1077.4$ Fg^{-1} at a high current density of 10.0 Ag^{-1}. Figure 7c shows the GCD plots of PANI/C/TiN NWA ternary nanocomposite at a current density of 1.0 Ag^{-1}. As seen from the figure, all these samples by having almost linear and symmetric curves demonstrated good electrochemical capacitance performance. The PANI/C/TiN NWA ternary nanocomposite presents a high specific capacitance of $C_{sp} = 1093$ Fg^{-1} at 1.0 Ag^{-1}. The specific capacitance of PANI/C/TiN NWA ternary nanocomposite remained at 98% of the initial specific capacitance after 2000 cycles. As a result, the good conductivity of electrode materials could facilitate high specific capacitance.

All the Nyquist plots corresponding to electrochemical impedance spectroscopy (EIS) consist of a nearly semicircle in the high frequency range and a straight line in the low frequency range as shown in Fig. 8a–c. As it is evident in all parts of Fig. 8, the EIS parameters, such as solution resistance (R_s) and charge transfer resistance (R_{ct}) in the high frequency region demonstrate that TiN-based composites are a favorable electrode with enhanced electronic conductivity and charge transport. At higher frequencies, the electrolyte ions do not penetrate into microporous structures. However, at low frequency regions, total impedance shows basically a capacitive behavior due to low diffusion of the electrolytes. At high frequency region, it is so fast and thus the ohmic resistance of microporous increases, which causes higher capacitance and hinders the migration of electrolytes in pores [130].

In literature, there are many TiN-based nanocomposites, which were presented in various electrolytes and specific capacitances as given in Table 2. The highest specific capacitance was obtained for PPy/TiN nanocomposite as $C_{sp} = 1265$ Fg^{-1} by GCD method at 0.6 Ag^{-1} in 1 M H_2SO_4 solution. TiN nanoparticles onto titanium foil were prepared

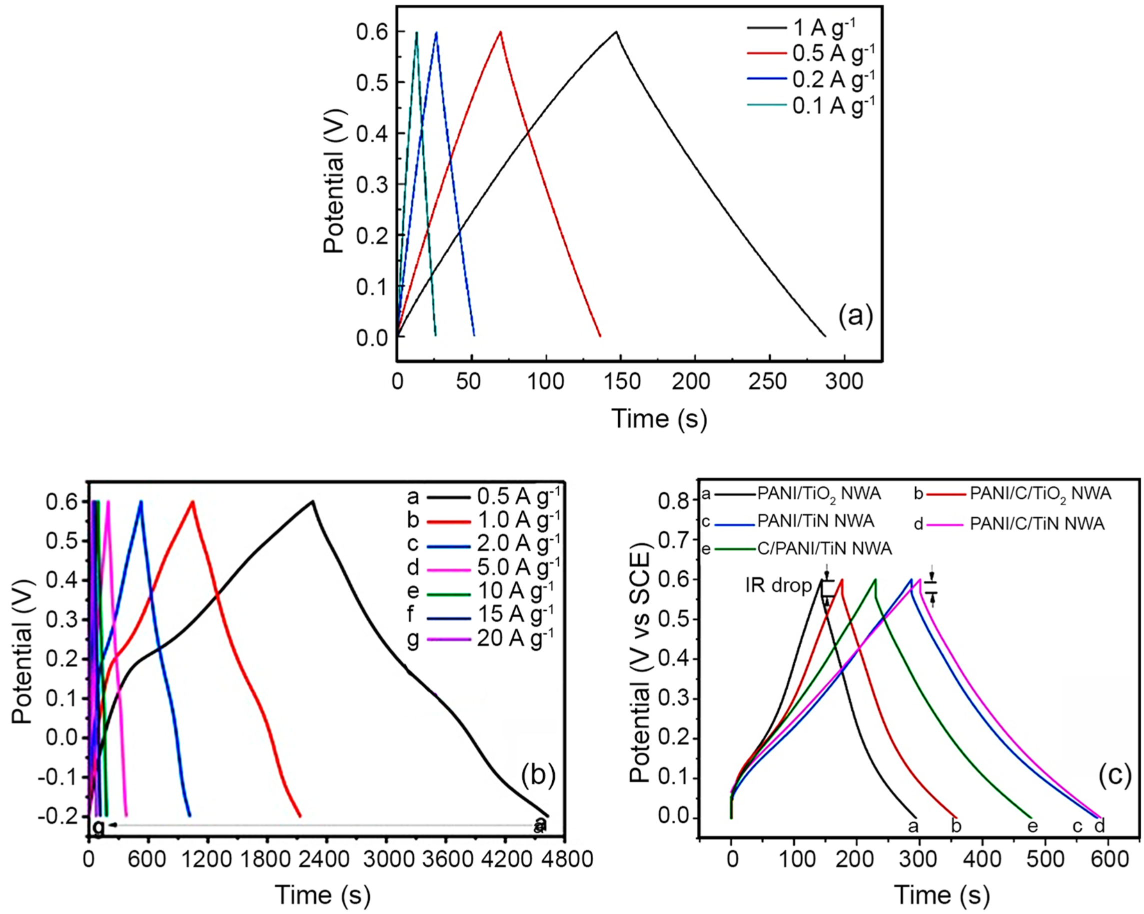

Fig. 7 Galvanostatic charge/discharge (GCD) graphs of **a** CL-TiN [125], **b** TiN/$NiCo_2O_4$ [126], **c** PPy/TiN/PANI [127], and **d** PANI/C/TiN NWA [128]. Reprinted with permission from Refs. [125–128]. Copyright: Elsevier (Refs. [125–128])

by potentiostatic electrolysis at + 5 V in an ammoniacal solution of potassium chloride (KCl) [131. A symmetric supercapacitor electrode showed a specific capacitance of C_{sp} = 44.10 $mFcm^{-2}$ at 6.66 $mAcm^{-2}$ in a good capacity retention (95% after 10,000 charge/discharge cycles) with ~ 100% coulombic efficiency (see Table 3).

Su et al. [138] have studied vanadium nitride (VN), which shows the capacitance of C_{sp} = 447.28 $mFcm^2$ at 2 $mAcm^{-2}$. Vanadium nitride/molybdenum disulfide (VN/MoS_2) hybrid composite reaches C_{sp} = 3187.3 $mFcm^2$, which is 7 times higher than C_{sp} of VN. Porous TiN electrode was coated on silicon substrate by direct current reactive sputtering method [139].

Titanium dioxide-based composites

Carbon/TiO_2-based supercapacitor

Carbon-based materials have more advantageous, such as closed-spaced carbon atoms, high strength, high electron density, and ultrahigh structure. There are many carbon materials, such as graphene, carbon fiber, carbon nanotube, fullerene, carbon black, etc. [140]. Graphene enables the decreasing rate of recombination of electron hole pairs through π–π interaction, and increases the charge transfer rate of the electrons [141].

Synthesis of carbon/TiO_2

The schematic synthetic procedure diagrams of titanium dioxide/*N*-doping graphene (*N*-TiO_2/NG) [142], TiO_2/graphene hydrogels [143], TiO_2/carbon nanofiber [144], rGO/TiO_2 [145] and rGO/thorn-like TiO_2 [146] are demonstrated in Fig. 9.

Capacitance results of carbon/TiO_2

Figure 10a presents the CV plots of *N*-TiO_2/NG electrode carried out at different scan rates from 1 to 50 mVs^{-1}, at a sweep potential of − 0.2 to 0.8 V in 1 M Na_2SO_4 solution. The CV plots indicate that the capacitance is mainly

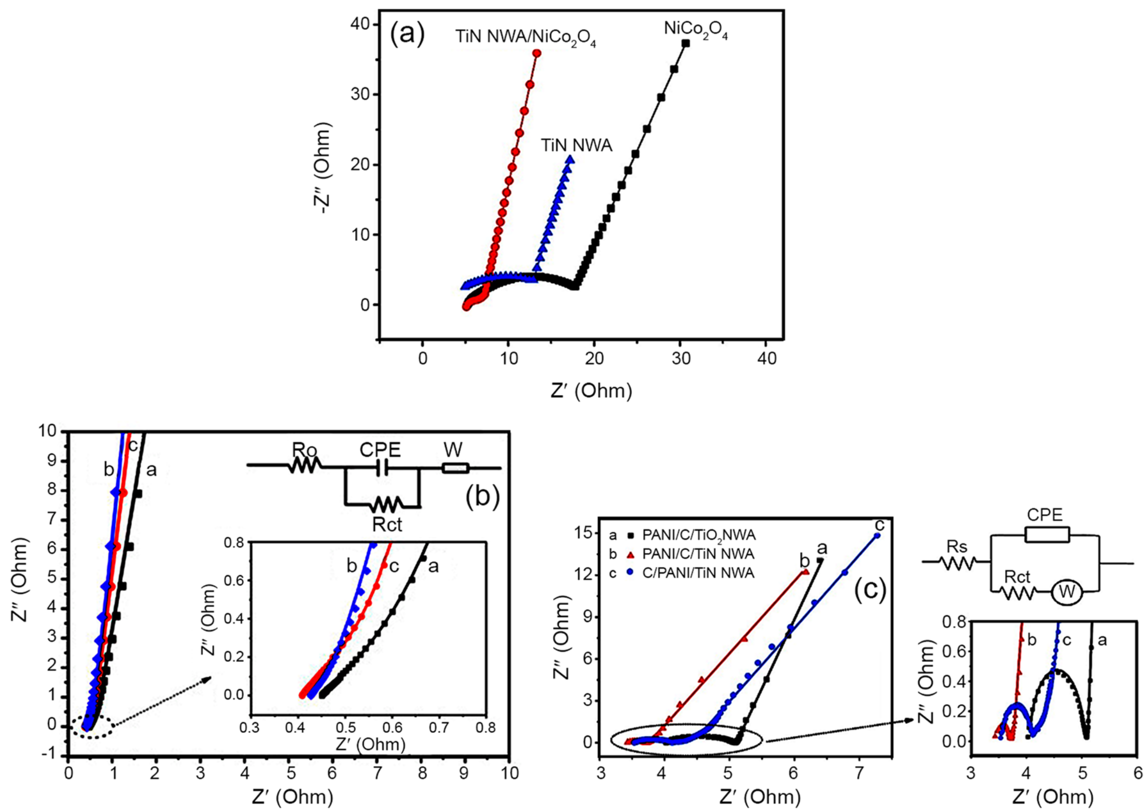

Fig. 8 Nyquist plots of **a** TiN/$NiCo_2O_4$ [126], **b** PPy/TiN/PANI [127], and **c** PANI/C/TiN NWA [128]. Reprinted with permission from Refs. [98–100]. Copyright: Elsevier (Refs. [126–128])

Table 2 Capacitance results of TiN-based materials

Materials	Electrolyte	Capacitance	References
PPy-TİN	1 M H_2SO_4	1265 Fg^{-1} at 0.6 Ag^{-1}	[132]
G/TİN	1 M KOH	333.7 Fg^{-1} at 1 Ag^{-1}	[133]
PANI/TİN core–shell	1 M H_2SO_4	1064.5 Fg^{-1} at 1 Ag^{-1}	[134]
TİN/C	6 M KOH	159 Fg^{-1} at 0.5 Ag^{-1}	[135]
TİN/VN	1 M KOH	170 Fg^{-1} at 2 mVs^{-1}	[136]
TiVN	1 M H_2SO_4	69.6 Fg^{-1} at 5 mVs^{-1}	[137]

created from the electric double layer capacitance (EDLC) behavior. Moreover, the redox peaks are also observed in the CV curves, which may be referred to pseudocapacitance. In addition, the highest specific capacitance of *N*-TiO_2/NG electrode was obtained as $C_{sp} = 205.1\ Fg^{-1}$ at 1 mVs^{-1}. The CV plots of the TiO_2/graphene hydrogels electrode measured in a three-electrode system in 1 M H_2SO_4 as electrolyte at a scan rate of 100 mVs^{-1} and voltage range between -0.4 and 0.6 V are given in Fig. 10b. The CV plots of the TiO_2/graphene hydrogel electrode showed a more quasi-rectangular shape and larger integral area related to a typical capacitive behavior as compared to other electrodes. The specific capacitance of electrode was calculated as $C_{sp} = 332.6\ Fg^{-1}$ at a current density of 0.2 Ag^{-1}. The CV curves of titanium dioxide/carbon nanofibers (TiO_2/CNFs) nanocomposite were performed in 6 M KOH electrolyte solution at a scan rate from 5 to 200 mVs^{-1} with a potential range of – 0.9 to 0 V. As it is given in Fig. 10c, the rectangular area increases with the scan rate of TiO_2/CNFs electrode, indication of an increase of electrode capacitance. In literature there are many studies using carbon nanotube (CNT) and graphene [147, 148]. Combining sulfur (S) with carbon-based materials and conducting polymers improves the electrochemical performances and electrical conductivity of electrode [149]. The cyclic voltammetry plots of the CNT/TiO_2 were obtained in 1 M phosphoric acid (H_3PO_4) solution at different scan rates in the voltage window from 0 to 1.4 V. The CV curves of rGO/TiO_2 nanocomposite electrode in 1 M H_2SO_4 electrolyte solution are illustrated in Fig. 10d. The CV graphs have a good rectangular box shape as seen from the figure. The rGO/TiO_2 nanocomposite electrode has the highest specific capacitance of $C_{sp} = 409.34\ Fg^{-1}$ at 4 mVs^{-1}. Figure 10e exhibits the CV curves of a rGO/thorn-like TiO_2 electrode, the three-electrode system, in 1 M Na_2SO_4 electrolyte solution for the potential window

Table 3 Some examples of TiO_2-based nanocomposites

Electrode	Electrolyte	Potential window /V	Specific capacitance/Fg^{-1}	Power density/$kWkg^{-1}$	Energy density/$Whkg^{-1}$	Cycling retention	References
Few layer Ti_3C_2/Ni foam	1 M Li_2SO_4	– 0.9, – 0.3	370 at 2 mVs^{-1}	–	–	86.3% after 10,000 cycles	[103]
PANI/TiO_2//$Ti_3C_2T_x$	1 M KOH	– 0.3, – 1	188 at 10 mVs^{-1}	–	–	94% after 8000 cycles	[109]
CL-TiN	1 M Na_2SO_4/CMC gel	0.0, 0.6	23.35	–	–	36.7% after 20.000 cycles	[125]
N-TiO_2/NG	1 M Na_2SO_4	– 0.2, + 0.8	205.1	–	–	78.8% after 5000 cycles	[142]
rGO/TiO_2	1 M H_2SO_4	0.0, 0.8	524.02	58.6	50.07	83.4% after 1000 cycles	[145]
Ag/TiO_2-NT	Different Ag ions	– 0.2, 0.6	86.9 mFg^{-1}	150.4 μWg^{-1}	82.8 μWhg^{-1}	–	[152]
V_2O_5/TiO_2	2 M HCl	– 0.2, 0.8	587	399 Wkg^{-1}	100.8	92% after 5000 cycles	[155]

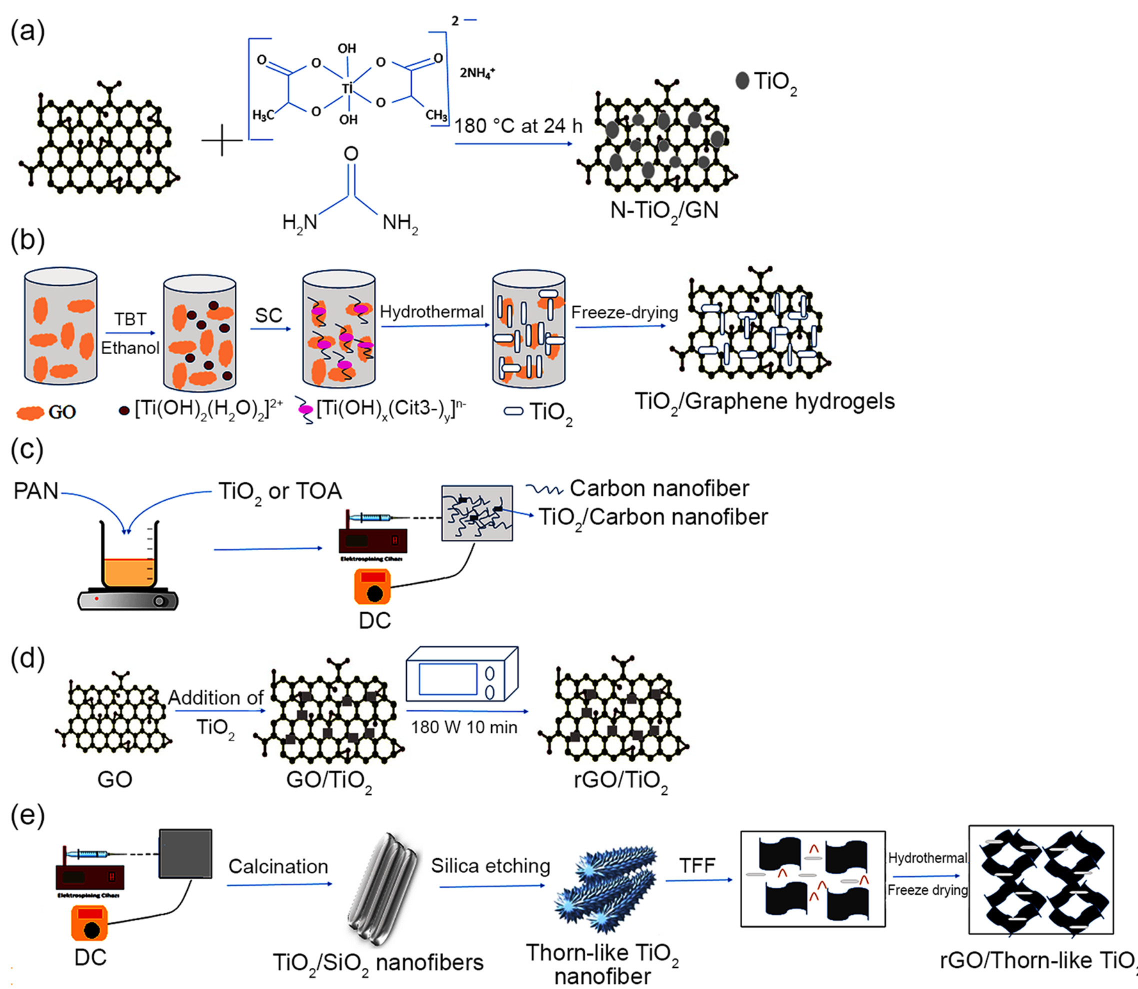

Fig. 9 Synthesis procedure of **a** *N*-TiO_2/NG [142], **b** TiO_2/graphene hydrogels [143], **c** TiO_2/carbon nanofiber [144], **d** rGO/TiO_2 [145], and **e** rGO/thorn-like TiO_2 [146]. Reprinted with permission from Refs. [142–146]. Copyright: Elsevier (Refs. [142–146])

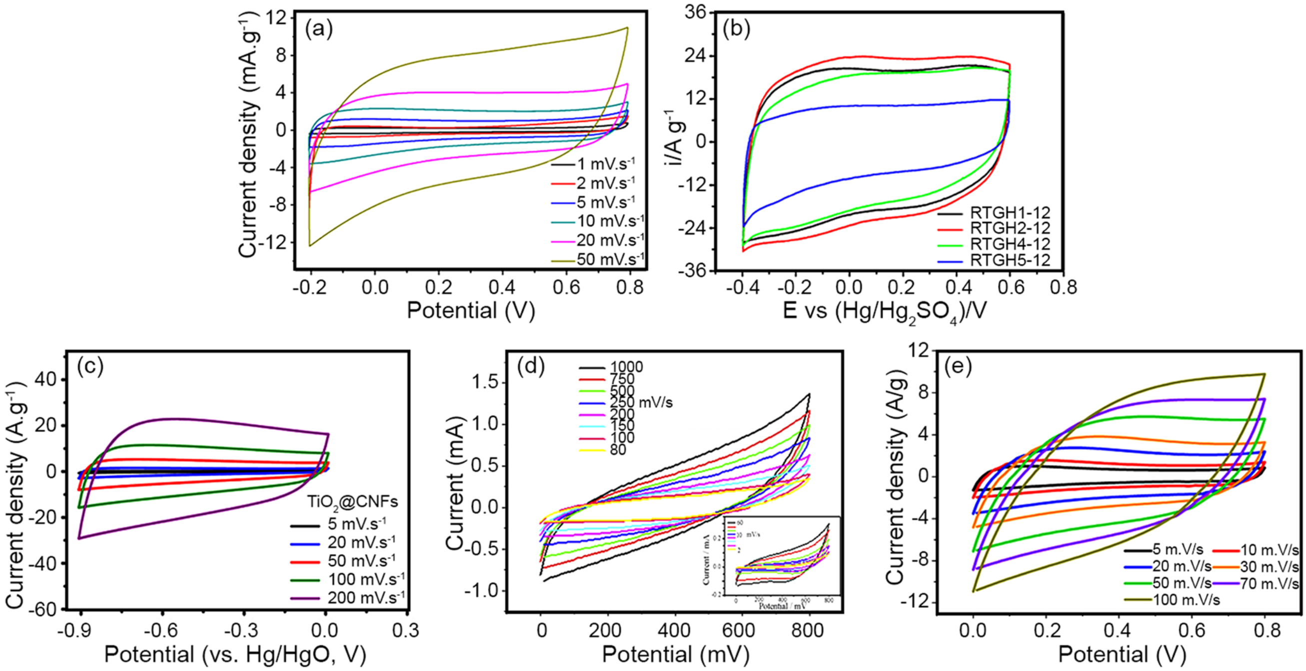

Fig. 10 CV graphs of **a** *N*-TiO_2/NG [142], **b** TiO_2/graphene hydrogels [143], **c** TiO_2/carbon nanofiber [144], **d** rGO/TiO_2 [145], and **e** rGO/thorn-like TiO_2 [146]. Reprinted with permission from Refs. [142–146]. Copyright: Elsevier (Refs. [142–146])

of 0–0.8 V at various scan rates from 5 to 100 mVs^{-1}. As it is evident from Fig. 10e, the area defined by the CV curve demonstrates an almost rectangular-box shape and it increases with increasing scan rate, indicating that the rGO/thorn-like TiO_2 electrode has low contact resistance and high quality capacitance behavior. The specific capacitance value of rGO/thorn-like TiO_2 electrode is computed to be $C_{sp} = 178$ Fg^{-1} at 1 Ag^{-1}.

The GCD measurements of *N*-TiO_2/NG nanocomposite were performed at a constant current density of 0.1, 0.5, 1, and 2 Ag^{-1}. The GCD curves of *N*-TiO_2/NG nanocomposite are given in Fig. 11a. It can be clearly seen from Fig. 11a that the longer discharging time of *N*-TiO_2/NG has higher capacitance than that of TiO_2/rGO nanocomposite. The electrical conductivity of graphene enhances due to the responsibility of the pyrrolic nitrogen and pyridinic nitrogen for nitrogen doping process. Figure 11b shows the GCD curves of TiO_2/graphene hydrogels electrode. As it is seen in the figure, the discharge plots of TiO_2/graphene hydrogels electrode have nearly symmetric behavior for the current density range of 0.2–8 Ag^{-1}. Therefore, the highest specific capacitance was obtained as $C_{sp} = 372.3$ Fg^{-1} at a current density of 0.2 Ag^{-1}. This indicates that the capacitive reversibility of the TiO_2/graphene hydrogels electrode is high. The charge and discharge curves of TiO_2/carbon nanofiber electrode are presented in Fig. 11c. The GCD curves of TiO_2/carbon nanofiber electrode are shown symmetrically and are similar to the isosceles triangle as seen from Fig. 11c. This refers to highly efficient and reversible progress of charge and discharge. The specific capacitance of TiO_2/carbon nanofiber was calculated to be $C_{sp} = 280.3$ Fg^{-1} at 1 Ag^{-1}. The galvanostatic charge/discharge curve of rGO/TiO_2 at a constant current density of 2 mA in a two-electrode configuration is presented in the literature [116]. The specific capacitances of rGO/TiO_2 electrode were computed as $C_{sp} = 24.84$ Fg^{-1}. Figure 11d shows the GCD curves of rGO/thorn-like TiO_2 electrodes. The specific capacitance of rGO/thorn-like TiO_2 nanocomposite electrode was calculated as $C_{sp} = 178$ Fg^{-1} at 1 Ag^{-1} from the slope of the GCD graph.

The Nyquist plots of *N*-TiO_2/NG are given in Fig. 12a. The Nyquist plots of *N*-TiO_2/NG show that the specific capacitance does not drop much even at higher current density, indicating that the electroactive materials have a good rate capacity. Figure 12b demonstrates the Nyquist plots of TiO_2/graphene hydrogels supercapacitor (SC). As given in the insert of Fig. 12b, the straight line associated with TiO_2/graphene hydrogels electrode is closer to the imaginary impedance axis in addition to a small semicircular curve. This verifies the superior ion diffusion efficiency of the device. The Nyquist plots corresponding to the EIS of TiO_2/carbon nanofiber are shown in Fig. 12c. The series resistance (R_t) for TiO_2/carbon nanofiber cathode and anode is calculated as 1.13 and 1.10 Ω, respectively. The EIS results of TiO_2/carbon nanofiber cathode and anode indicated good stability and reversibility of this symmetric two-electrode supercapacitor. Figure 12d presents the Nyquist plots of

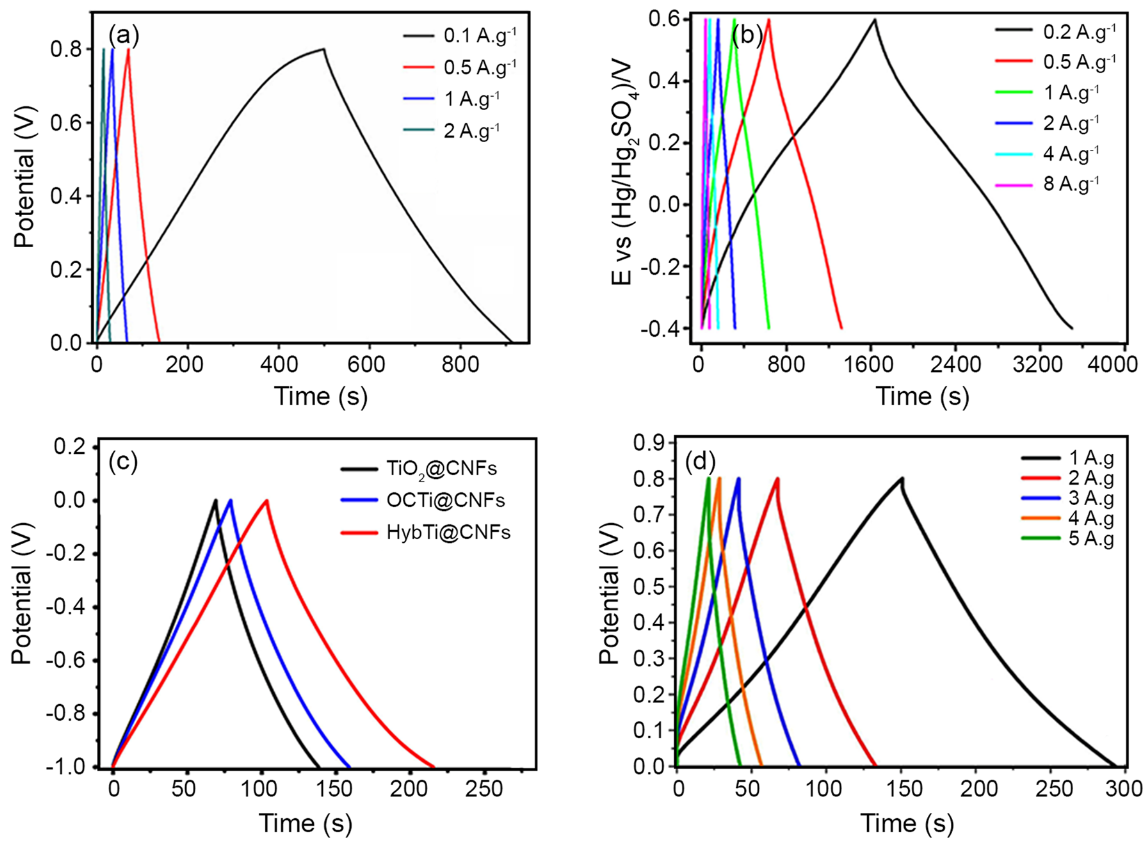

Fig. 11 Galvanostatic charge/discharge (GCD) graphs of **a** *N*-TiO_2/NG [142], **b** TiO_2/graphene hydrogels [143], **c** TiO_2/carbon nanofiber [144], **d** rGO/TiO_2 [145], and **e** rGO/thorn-like TiO_2 [146]. Reprinted with permission from Refs. [113–117]. Copyright: Elsevier (Refs. [142–146])

rGO/TiO_2 electrode using a sinusoidal signal at 0 V in a frequency range from 10 mHz to 100 kHz with 10 mV amplitude. Relating to rGO, impedance spectra involve a semicircle part, representing to the carrier transport process and a linear part, representing to the diffusion process. The diameter of the semicircle curve presents the charge transfer resistance (R_{ct}) at the electrode surface. The Nyquist plots of rGO/TiO_2 electrode indicate to low R_{ct} and good conductivity.

Metal/TiO_2-based supercapacitor

Synthesis of metal/TiO_2

Metal or metal oxide-based electrode materials have multiple active sites used in supercapacitors [150]. Iqbal et al. [151] have synthesized strontium oxide (SrO) from sonochemical method by calcination. The synthetic procedure of silver/titanium dioxide (Ag/TiO_2) nanotubes [152], manganese (IV) oxide/titanium dioxide (MnO_2/TiO_2) nanotube arrays [153], α-molybdenum oxide nanoplate/titanium dioxide (α-MoO_3 nanoplate/TiO_2) [154] and vanadium pentaoxide/titanium dioxide (V_2O_5/TiO_2) nano-arrays [155] is presented in Fig. 13.

Capacitance results of metal/TiO_2

The CV measurements of Ag/TiO_2 nanotube electrode were carried out at different scan rates in the voltage range from − 0.2 to + 0.6 V. The CV plots of Ag/TiO_2 nanotubes are illustrated in Fig. 14a. As seen from this figure, the increasing in scan rate has not changed the shape of the basic CV curve. The Ag/TiO_2 nanotubes electrode still keeps a good rectangular box shape with a larger integral area at a high scan rate of 100 mVs^{-1}. The large specific capacitance value after modified ion implantation demonstrates an improvement in the electrochemical performance. The CV plots of MnO_2/TiO_2 nanotube arrays are presented in Fig. 14b for various scan rates with a three-electrode system in 0.5 M Na_2SO_4 electrolyte. The CV areal capacitance of MnO_2/TiO_2 nanotube was obtained as C_{sp} = 346.5 $mFcm^{-2}$ at 5 mVs^{-1}. The electrochemical measurements were performed with a three-electrode system in 1 M Na_2SO_4 electrolyte to figure out the electrochemical performance of the α-MoO_3 nanoplate/TiO_2

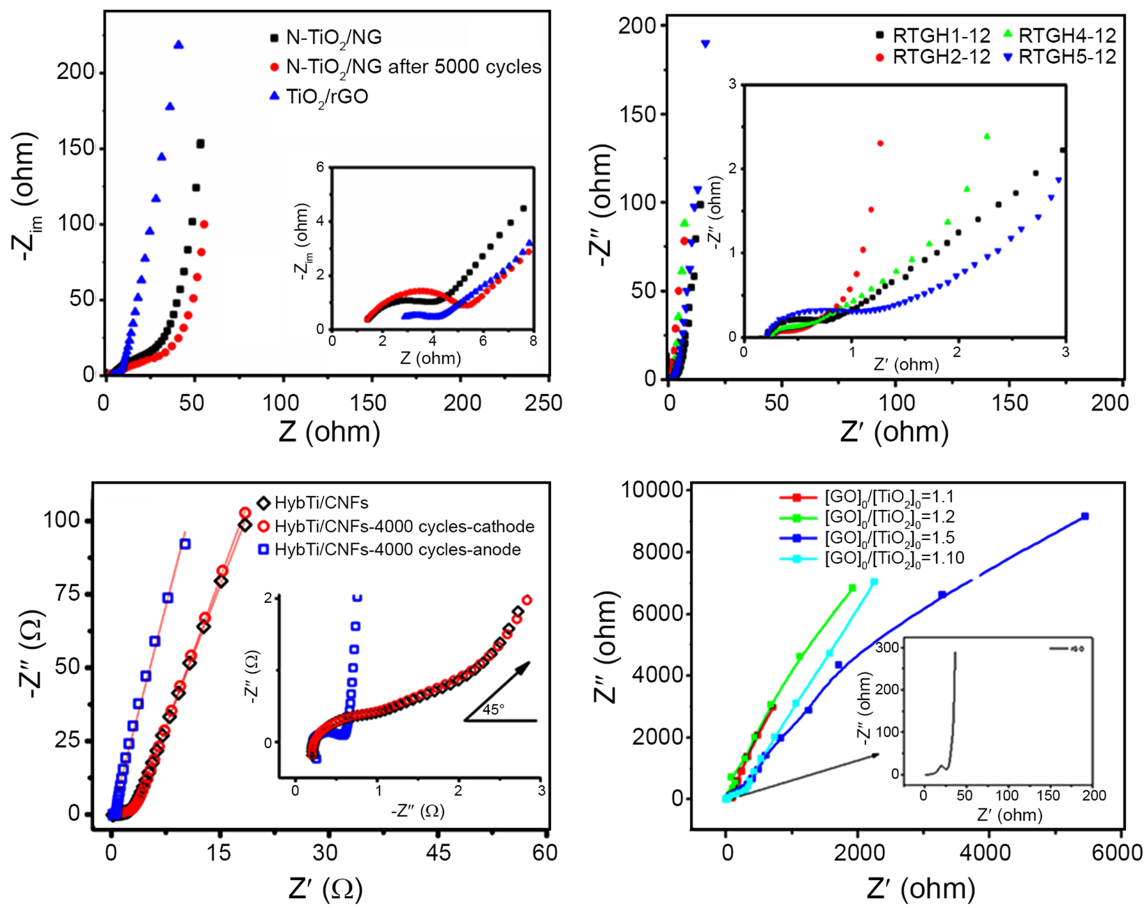

Fig. 12 Nyquist plots of **a** *N*-TiO_2/NG [Ti 142], **b** O_2/graphene hydrogels [143], **c** TiO_2/carbon nanofiber [144], and **d** rGO/TiO_2 [145]. Reprinted with permission from Refs. [142–145]. Copyright: Elsevier (Refs. [142–145])

electrode. The effect of different scan rates on the electrochemical behavior of α-MoO_3 nanoplate/TiO_2 electrode is presented in Fig. 14c. All CV plots are close to an ideal rectangular box-shape with no evidence of redox peaks. In other words, the device shows a typical character of double-layer capacitance behaviour. Moreover, the CV plots did not dramatically change when the scan rate increased to 0.2 Vs^{-1}. The CV measurements of 3D-TiO_2/1D-TiO_2 nanotube electrode material were studied by a conventional three-electrode system with 1 M potassium hydroxide (KOH) and recorded at different scan rates (5–50 mVs^{-1}). The cyclic voltammetry (CV) curves of V_2O_5/TiO_2 nano-arrays electrode measured at different scan rates from 5 to 100 mVs^{-1} are given in Fig. 14d. The areas of CV curves expand accordingly while their shapes stay well with the increasing of the scan rate. This result indicates an ideal capacitive behavior of V_2O_5/TiO_2 nano-arrays electrode with ion diffusion and fast charge rate as seen from Fig. 14d. The quasi-rectangular shape of the CVs was obtained, indicating an ideal supercapacitive material with good interfacial kinetic and high-rate performance. The highest specific capacitance value was calculated as $C_{sp} = 587\ Fg^{-1}$ at current density of 0.5 Ag^{-1}.

The galvanostatic charge/discharge (GCD) curves of Ag/TiO_2 nanotubes electrode are given in Fig. 15a. The charge and discharge curves may indicate that Ag/TiO_2 nanotubes electrode exhibits a good symmetry and linear properties under different current densities as it is seen in Fig. 15a. That means that the Ag/TiO_2 nanotube electrode has a high coulombic efficiency. Futhermore, the Ag/TiO_2 nanotube electrode has a high specific capacitance as $C_{sp} = 9324.6$ $mFcm^{-3}$ (86.9 mFg^{-1} or 1.2 $mFcm^{-2}$) at the current density of 0.05 $mAcm^{-2}$. The GCD measurements of MnO_2/TiO_2 nanotube arrays electrode were carried out at different current densities of 0.1, 0.5, 1.0, 2.0, 3.0, 4.0 and 10.0 $mAcm^{-2}$. The charge and discharge curves of MnO_2/TiO_2 nanotube arrays electrode are shown in Fig. 15b. As it is evident in this figure, with the increasing current density, all the GCD curves have a level. The potential of the charging level increases while the potential of the discharging level decreases due to the level potential of the pseudocapacitive material caused by the creation or annihilation of electrons.

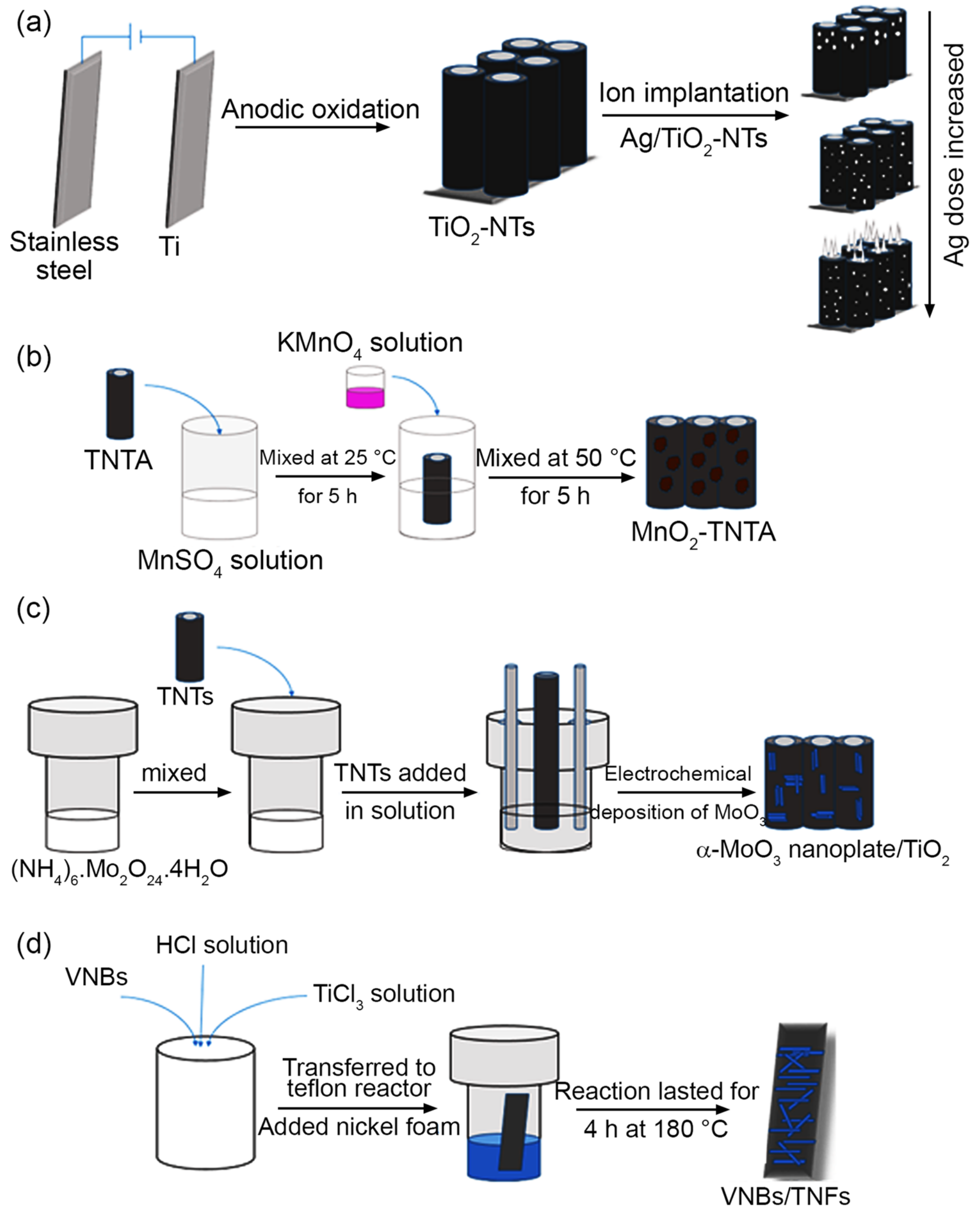

Fig. 13 Synthesis procedure of **a** Ag/TiO_2 nanotubes [152], **b** MnO_2/TiO_2 nanotube arrays [153], **c** α-MoO_3 nanoplate/TiO_2 [154], and **d** V_2O_5/TiO_2 nano-arrays [155]. Reprinted with permission from Refs. [152–155]. Copyright: Wiley (Ref. [152]), Copyright: Elsevier (Ref. [153]), Copyright: Springer (Ref. [154]), Copyright: Royal Society of Chemistry (Ref. 155)

Moreover, the areal capacitance values of MnO_2/TiO_2 nanotube arrays electrode were calculated as C_{sp} = 436.2, 370.3, 281.7, 151.4, 84.3, 47.5, and 32.7 mFcm^{-2} for the current densities of 0.1, 0.5, 1.0, 2.0, 3.0, 4.0, and 10.0 mAcm^{-2}, respectively. Figure 15c demonstrates the GCD curves of α-MoO_3 nanoplate/TiO_2 electrode with the current densities between 0.4 and 1 mAcm^{-2}. The inner active sites or the pores of the α-MoO_3 nanoplate/TiO_2 electrode are fully accessible and propagated by cations at low current densities. Hence, the highest areal capacitance was found as C_{sp} = 42.89 mFcm^{-1} at a current density of 0.6 mAcm^{-1}. Figure 15d shows the GCD curve of symmetrical cell with a V_2O_5/TiO_2 nano-arrays electrode. The highest specific capacitance of V_2O_5/TiO_2 nano-arrays electrode is found as C_{sp} = 287 Fg^{-1} at the current densities of 0.5 Ag^{-1}.

The Nyquist plots corresponding to the EIS of Ag/TiO_2 nanotubes electrode in 0.5 M Na_2SO_4 solution are shown in Fig. 16a. In this figure, the diameter of semicircle is small at its high-frequency zone and straight line is close to 90° at its low-frequency area. These results indicate that the internal resistance of Ag/TiO_2 nanotubes electrode is very small and the electrode has a very good capacitance performance, respectively. Moreover, the charge transfer resistance value of Ag/TiO_2 nanotubes electrode was computed as R_{ct} = 74.79 Ωcm^2. Figure 16b demonstrates the Nyquist plots of MnO_2/TiO_2 nanotube arrays electrode. The electrochemical impedance spectroscopy of MnO_2/TiO_2 nanotube arrays points out that the reaction of electrode mainly involves the charge transfer process and ion diffusion. According to the Nyquist curve of MnO_2/TiO_2 nanotube arrays given in Fig. 16b, the

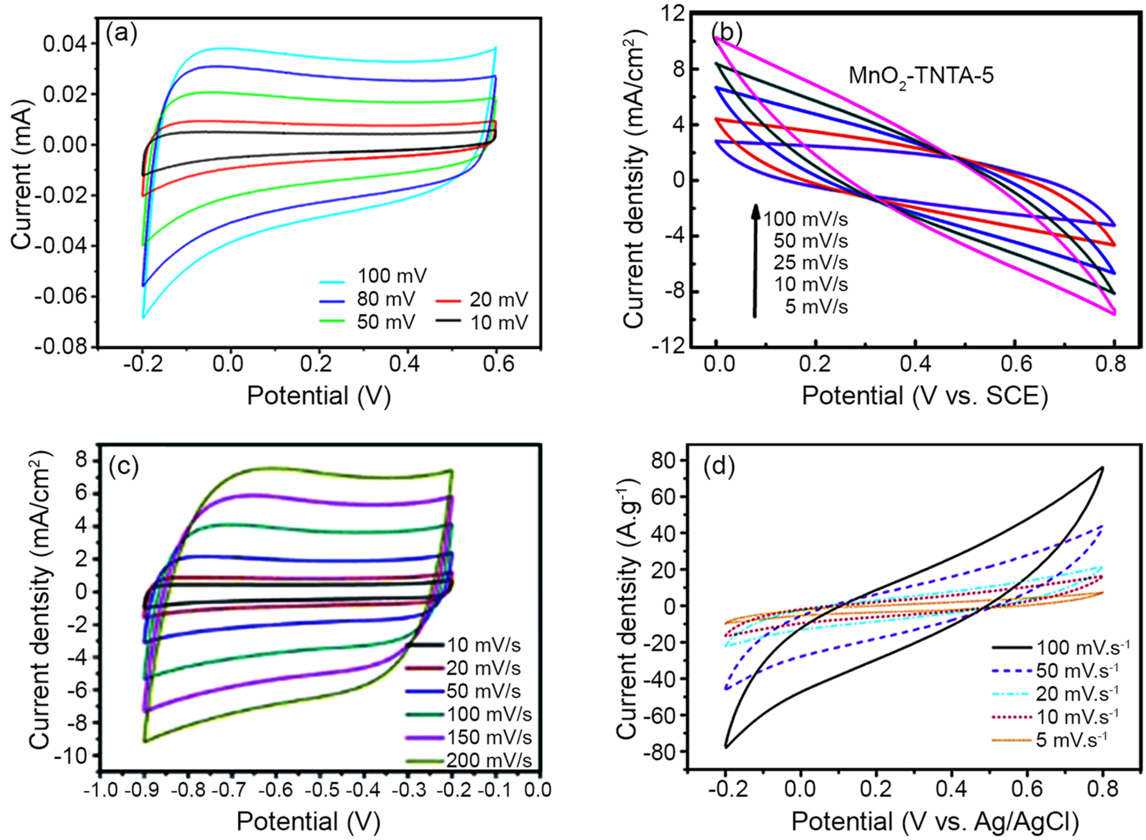

Fig. 14 CV graphs of **a** Ag/TiO_2 nanotubes [152], **b** MnO_2/TiO_2 nanotube arrays [153], **c** α-MoO_3 nanoplate/TiO_2 [154], and **d** V_2O_5/TiO_2 nano-arrays [155]. Reprinted with permission from Refs. [152–155]. Copyright: Wiley (Ref. [152]), Copyright: Elsevier (Ref. [153]), Copyright: Springer (Ref. [154]), Copyright: Royal Society of Chemistry (Ref. [155])

MnO_2/TiO_2 nanotube arrays electrode has the charge transfer resistance of $R_{ct} = 73.8\ \Omega cm^2$. The electrochemical impedance spectroscopy of α-MoO_3 nanoplate/TiO_2 electrode is presented in Fig. 16c. The semicircular curves which are seen in the Nyquist plots of electrodes indicate that the electrodes have a poor charge transfer performance because of the interlayer transfer resistance between the electrode and electrolyte systems. However, there is no such semicircular curve for the α-MoO_3 nanoplate/TiO_2 electrode as given in Fig. 16c. This result indicates to a good charge transport capability and better capacitance performance of the α-MoO_3 nanoplate/TiO_2 electrode. Figure 16d presents the Nyquist plots of V_2O_5/TiO_2 nano-arrays electrode. The charge transfer resistance (R_{ct}) of V_2O_5/TiO_2 nano-arrays electrode was calculated from the diameter of semicircle curve as 2.6 Ω. The small charge transfer resistance and the ion transportation/diffusion resistance of V_2O_5/TiO_2 nano-arrays electrode demonstrate that TiO_2 can increase the active surface and supply fast channels for insertion of ions in and out of the electrode material. Nickel/metal–organic framework (Ni/MOF)-derived mesoporous carbon was synthesized by carbonization and acid treatment [156]. The tubular Co_3O_4 showed good electrochemical performance in 3 M KOH solution ($P = 5500$ Wkg^{-1} and $E > 22$ $Whkg^{-1}$) [157]. Cobalt molybdate ($CoMoO_4$) electrode shows a specific capacitance of $C_{sp} = 294$ Fg^{-1} by CV method with $E = 7.3$ $Whkg^{-1}$ and $P = 7227.5$ Wkg^{-1} [158].

Conducting polymer/TiO_2-based supercapacitor

Synthesis of conducting polymer/TiO_2 nanocomposite

Synthesis procedure of PANI/TiO_2 nanocomposite [159] is given in Fig. 17. Chemical polymerization was performed by ammonium persulfate as an initiator.

Different types of conducting polymers have been used as surface modifiers [160]. These conducting polymers are polyaniline (PANI) [161–163], polypyrrole (PPy) [164, 165], polythiophene (PTh) [166], poly(3,4-ethylenedioxythiophene) (PEDOT) [167, 168], etc. In literature, PANI–TiO_2–GO composites have been presented by Phan et al. [169]. In this work, the chemical method was performed in a paste form on titanium substrate. A TiO_2-coated multiwalled carbon nanotubes (MWCNT)/graphene/PANI

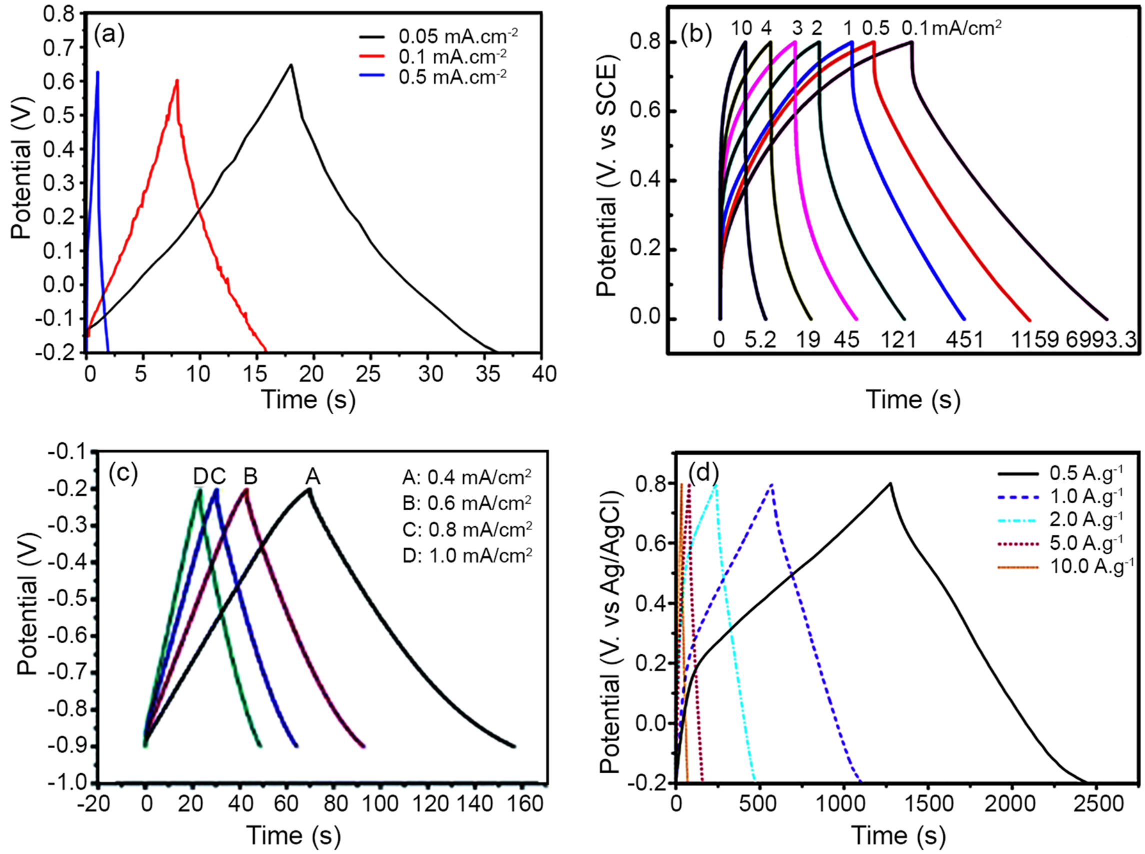

Fig. 15 Galvanostatic charge/discharge (GCD) graphs of **a** Ag/TiO_2 nanotubes [152], **b** MnO_2/TiO_2 nanotube arrays [153], **c** α-MoO_3 nanoplate/TiO_2 [154], and **d** V_2O_5/TiO_2 nano-arrays [155]. Reprinted with permission from Refs. [152–155]. Copyright: Wiley (Ref. [152]), Copyright: Elsevier (Ref. [153]), Copyright: Springer (Ref. [154]), Copyright: Royal Society of Chemistry (Ref. [155])

nanocomposite was studied for supercapacitor applications [170]. The specific capacitance value of TiO_2-coated MWCNT in a weight ratio of (9:1) was obtained as $C_{sp} = 666.3\ Fg^{-1}$ at 2 mVs^{-1}.

Capacitance results of conducting polymer/TiO_2 nanocomposite

The CV measurements of PANI/TiO_2 nanocomposite electrode were carried out in 1 M H_2SO_4 solution at different scan rates. Figure 18a presents the CV curves of PANI/TiO_2 nanocomposite electrode. During the redox process, the charges in the electrolyte inside the electrode are depleted or saturated due to the slow charge transfer process at high scan rate. This usually results in increased ionic resistivity, which leads to a drop in the capacitance of the electrode.

The galvanostatic charge–discharge curves of PANI and PANI/TiO_2 nanocomposite electrode are shown in Fig. 18b inset 1 and Fig. 18b inset 2, respectively. The GCD measurements of PANI/TiO_2 nanocomposite were performed in the potential range of – 0.2 to + 0.8 V versus saturated calomel electrode (SCE) with a constant current density of 0.5 $mAcm^{-2}$. As seen from Fig. 18b, the GCD curves of electrodes are not ideal straight lines indicating the faradaic reaction process. Moreover, there is an initial potential drop due to internal resistance, which comes from the resistance of both the electrode and the electrolyte. In addition, the highest specific capacitance was calculated as $C_{sp} = 783\ Fg^{-1}$ at 5 mVs^{-1} for PANI/TiO_2 nanocomposite.

The Nyquist plots of PANI (Fig. 18c inset 1) and PANI/TiO_2 (Fig. 18c inset 2) nanocomposite electrode in 1 M H_2SO_4 electrolyte are shown in Fig. 18c. The Nyquist plot of PANI/TiO_2 nanocomposite electrode is a semicircle at high frequencies and it is a line at low frequencies as observed in Fig. 18c. The semicircle corresponds to resistance due to charge transfer between geometric interfaces and geometric capacitance. The line observed at low frequencies is due to the charge transfer impedance resulting from the inhomogeneous concentration of the charged types in the material. Moreover, the electrochemical charge transfer resistance value of PANI/TiO_2 nanocomposite was calculated as 20 Ω. As a result, the electrochemical impedance spectroscopy analysis of PANI/TiO_2 nanocomposite demonstrated that this electrode is suitable to use at low frequency region. In

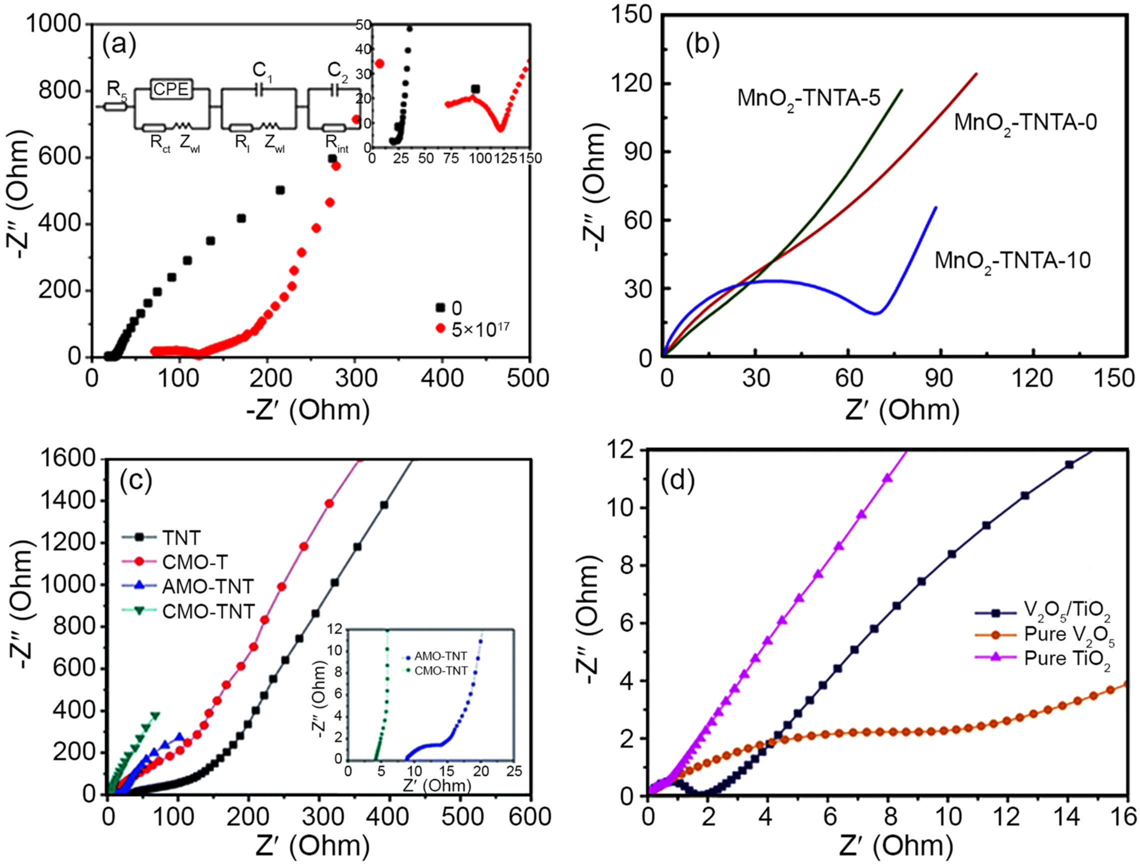

Fig. 16 Nyquist plots of **a** Ag/TiO_2 nanotubes [152], **b** MnO_2/TiO_2 nanotube arrays [153], **c** α-MoO_3 nanoplate/TiO_2 [154], and **d** V_2O_5/TiO_2 nano-arrays [155]. Reprinted with permission from Refs. [152–155]. Copyright: Wiley (Ref. [152]), Copyright: Elsevier (Ref. [153]), Copyright: Springer (Ref. [154]), Copyright: Royal Society of Chemistry (Ref. [155])

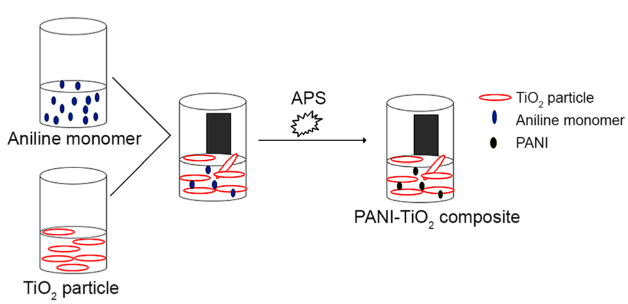

Fig. 17 Synthesis procedure of PANI/TiO_2 nanocomposite [159]. Reprinted with permission from Ref. [159]. Copyright: Royal Society of Chemistry (Ref. [159])

literature, TiO_2/PANI hybrid composites have been synthesized with different methods [171]. Furthermore, many conducting polymers/TiO_2 composites are presented in literature [172, 173]

Reduced graphene oxide (rGO) and its composites have mostly been used as an electrode material for supercapacitors due to their good electrical conductivity, high surface area, low cost, and high yield [174]. In literature, the given capacitance values for graphene–titanium dioxide/polythiophene (G-TiO_2/PTh), graphene–titanium dioxide (G-TiO_2) and graphene (G) are 162.5, 62.3, and 47.1 Fg^{-1}, respectively [175]. Li et al. synthesized alkoxy-functionalized polythiophene (PM4EOT) and TiO_2 nanocomposites by a facile in situ oxidative polymerization of thiophene monomer [176]. The specific capacitance of PM4EOT/TiO_2 nanocomposite (1:1) was given as $C_{sp} = 111$ Fg^{-1} at a current density of 0.5 Ag^{-1}.

Future perspectives of scientific trends and challenges

Cheaper and easily prepared and long cyclic life materials can be chosen in future energy storage devices. TiO_2 is one of the most important redox active materials used for these systems. It can be mostly used in solar photovoltaics [177], photo-electrochemical cells [178, 179], supercapacitors [180] and batteries [181]. Among the different types of energy storage systems, supercapacitors are of great interest due to their high specific capacitance, superior power density, eco-friendless, reversible character, and self-durability [182]. Supercapacitor cell performance can be evaluated by

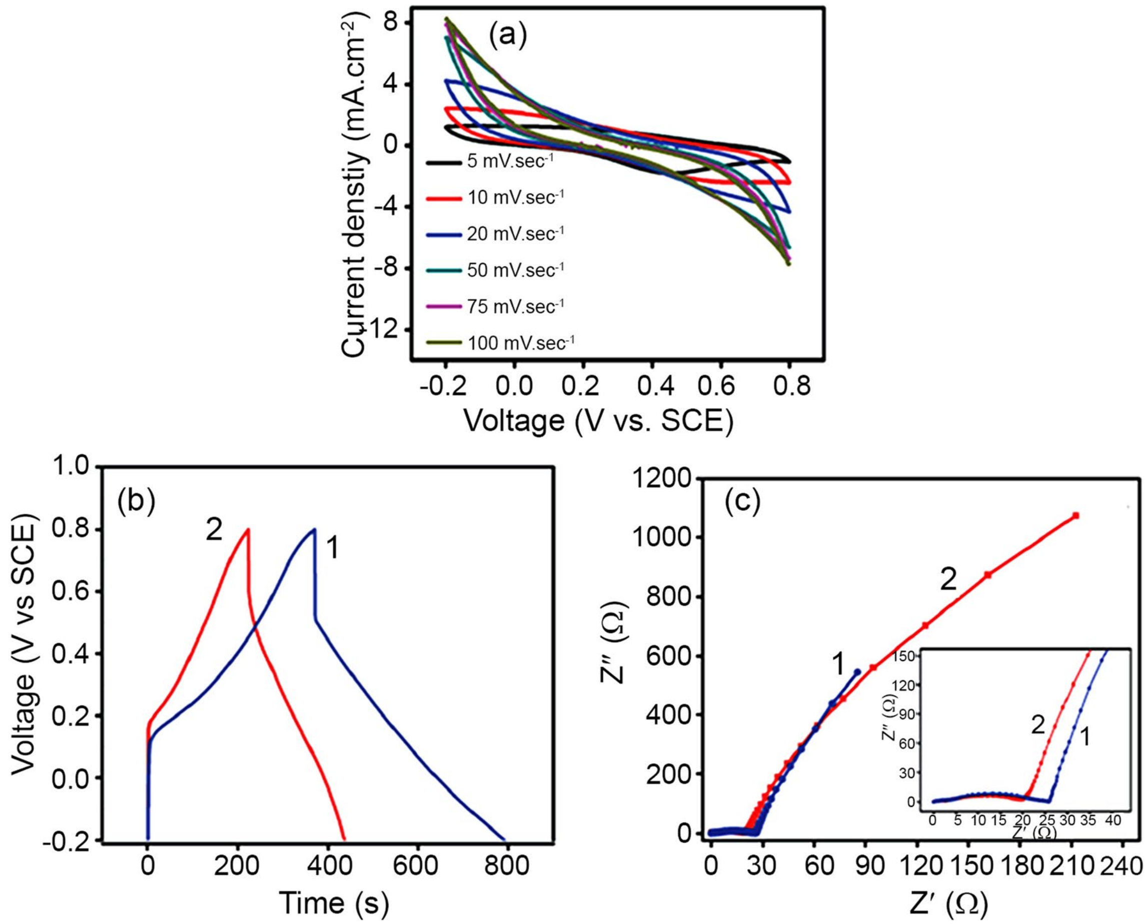

Fig. 18 **a** CV **b** GCD, and **c** Nyquist plots of PANI/TiO_2 nanocomposite [159]. Reprinted with permission from Ref. [159]. Copyrigh: Royal Society of Chemistry (Ref. [159])

many criteria, such as selection of electrolyte type, electrode type, separator type, chosen potential window, and used method and so on [140].

Conclusion

This paper has reviewed the research progress in the titanium-based materials for supercapacitor electrodes. Many techniques, such as synthesis procedure, CV, GCD, EIS, and equivalent circuit models were presented to explain in more detail as TiO_2-based materials in supercapacitor applications. The type of TiO_2-based nanocomposite which has higher specific capacitance and electrochemical performances (energy and power density or stability). Moreover, the factor which affects this nanocomposite material? This review article answers these important questions on the basis of TiO_2-based nanocomposites for supercapacitors. The following factors affect significantly on the supercapacitors, such as highly conductive materials, porous materials, and good diffusion pathways.

Titanium nitride (TiN) materials have higher electrical conductivity (4000–55,500 Scm^{-1}) as electrode materials for pseudocapacitors. Therefore, the PPy/TiN nanocomposite has the highest specific capacitance as $C_{sp} = 1265$ Fg^{-1} in the GCD method (0.6 Ag^{-1}) in 1 M H_2SO_4 solution. TiO_2-based materials have a positive effect and a synergy to increase electrochemical performance of supercapacitors. In addition, higher conductivite materials, such as TiN type materials and conducting polymers (π-conjugation process) supply higher electrochemical performance of supercapacitors. Since they can provide a variety of oxidation states for effiecient redox charge carriers.

Acknowledgements Financial support of this work is provided by TUBITAK, grant no: 117M042. The authors thank the TUBITAK MAG workers for their technical and financial supports.

Author contributions The manuscript was written through the contributions of all authors.

Declarations

Conflict of interest This paper consists of original study, unpublished work, which is not under consideration for publication elsewhere. The paper was approved to all authors and there is no conflict of interest for publication.

References

1. Choi NS, Chen ZH, Freunberger SA, Ji XL, Sun YK, Amine K, Yushin G, Nazar LF, Cho J, Bruce PG (2012) Challenges facing lithium batteries and electrical double layer capacitors. Angew Chem Int Ed 51:9994–19924
2. Wang JR, Vila N, Walcarius A (2020) Redox-active vertically aligned mesoporous silica thin films as transparent surfaces for energy storage applications. ACS Appl Mater Interfaces 12:24262–24270
3. Hu ZA, Xie YL, Wang YX, Xie LJ, Fu GR, Jin XQ, Zhang ZY, Yang YY, Wu HY (2009) Synthesis of alpha-cobalt hydroxides with different intercalated anions on their morphology, basal plane spacing, and capacitive property. J Phys Chem C 113:2502–2508
4. Ates M, El-Kady M, Kaner RB (2018) Three-dimensional design and fabrication of reduced graphene oxide/polyaniline composite hydrogels electrodes for high performance electrochemical supercapacitors. Nanotechnology 29:175402–175412
5. Zhou CA, Yao ZJ, Xia XH, Wang XL, Gu CD, Tu JP (2020) Low-strain titanium-based oxide electrodes for electrochemical energy storage devices: design, modification, and application. Mater Today Nano 11:100085
6. Li T, Li S, Zhang B, Wang B, Nie D, Chen Z, Yan Y, Wan N, Zhang W (2015) Supercapacitor electrode with a homogeneously Co_3O_4-coated multiwalled carbon nanotube for a high capacitance. Nanosc Res Lett 10:208
7. Bandgar SB, Vadigar MM, Jambhale CL, Kim JH, Kolekar SS (2021) Superfast ice crystal-assisted synthesis of $NiFe_2O_4$ and $ZnFe_2O_4$ nanostructures for flexible high-energy density asymmetric supercapacitors. J Alloys Compds 853:157129
8. Yan WK, Bi JQ, Wang WL, Xing Z, Liu R, Hao XX, Gao XC, Leng MZ (2021) Hierarchical MnO_2@$NiCo_2O_4$@Ti_3SiC_2/carbon cloth core shell structure with superior electrochemical performance of all solid-state supercapacitors. Ceram Int 47:292–300
9. Bu IYY, Huang R (2017) Fabrication of CuO decorated reduced graphene oxide nanosheets for supercapacitor applications. Ceram Int 43:45–50
10. Wang H, Yao CJ, Nie HJ, Yang L, Mei SL, Zhang QC (2020) Recent progress in integrated functional electrochromic energy storage devices. J Mater Chem C 8:15507–15525
11. Liu T, Yao TH, Li L, Zhu L, Wang JK, Li F, Wang HK (2020) Embedding amorphous lithium vanadate into carbon nanofibers by electrospinning as a high-performance anode material for lithium-ion batteries. J Colloid Interface Sci 580:21–29
12. Neira S, Pereda J, Rojas F (2020) Three-part full-bridge bidirectional converter for hybrid DC/DC/AC systems. IEEE Trans Power Electron 35:13077–13084
13. Liu JL, Zhang TR, Waterhouse GIN (2020) Complex alloy nanostructures as advanced catalysts for oxygen electrocatalysis: from materials design to applications. J Mater Chem A 8:23142–23161
14. Raza W, Ali F, Raza N, Luo Y, Kim KH, Yang J, Kumar S, Mehmood A, Kwon EE (2018) Recent advancements in supercapacitor technology. Nano Energy 52:441–473
15. Snook GA, Kao P, Best AS (2011) Conducting polymer based supercapacitor devices and electrodes. J Power Sources 196:1–12
16. Zhi MJ, Xiang CC, Li JT, Li M, Wu NQ (2013) Nanostructured carbon–metal oxide composite electrodes for supercapacitors: a review. Nanoscale 5:72–88
17. Nikokavoura A, Trapalis C (2017) Alternative photocatalysts to TiO_2 for the photocatalytic reduction of CO_2. Appl Surf Sci 391:149–174
18. Pal B, Vijayan BL, Krishnan SG, Harilal M, Basirun WJ, Lowe A, Yusoff MM, Jose R (2018) Hydrothermal syntheses of tungsten doped TiO_2 and TiO_2/WO_3 composite using metal oxide precursors for charge storage applications. J Alloys Compd 740:703–710
19. Ning P, Duan X, Ju X, Lin X, Tong X, Pan X, Wang T, Li Q (2016) Facile synthesis of carbon nanofibers/MnO_2 nanosheets as high-performance electrodes for asymmetric supercapacitors. Electrochim Acta 210:754–761
20. Ensafi AA, Ahmadi N, Rezaei B, Abdolmaleki A, Mahmoudian M (2018) A new quaternary nanohybrid composite electrode for a high-performance supercapacitor. Energy 164:707–721
21. Muzaffar A, Ahamed MB, Deshmukh K, Thirumalai J (2019) A review on recent advances in hybrid supercapacitors: design, fabrication and applications. Renew Sustain Energy Rev 101:123–145
22. Prasanna BP, Avadhani DN, Chaitra K, Nagaraju N, Kathyayini N (2018) Synthesis of polyaniline/MWCNTs by interfacial polymerization for superior hybrid supercapacitance performance. J Polym Res 25:123
23. Da Silva EP, Rubira AF, Ferreira OP, Silva R, Muniz EC (2019) In situ growth of manganese oxide nanosheets over titanium dioxide nanofibers and their performance as active material for supercapacitor. J Colloid Interface Sci 555:373–382
24. Mao H, Rasheed A (2018) Facile synthesis of porous Mn_2TiO_4/TiO_2 composites for high performance supercapacitors. Mater Lett 215:114–117
25. Zhao Y, Xu L, Huang S, Bao J, Qiu J, Lian J, Xu L, Huang Y, Xu Y, Li H (2017) Facile preparation of TiO_2/C_3N_4 hybrid materials with enhanced capacitive properties for high performance supercapacitors. J Alloys Compd 702:178–185
26. Ozalins V, Zhou F, Asta M (2013) Ruthenia-based electrochemical supercapacitors: insights from first-principles calculations. ACC Chem Res 46:1084–1093
27. Raccichini R, Varzi A, Passerini S, Scrosati B (2015) The role of graphene for electrochemical energy storage. Nat Mater 14:271–279
28. Hou J, Shao Y, Ellis MW, Moore RB, Yi B (2011) Graphene-based electrochemical energy conversion and storage: fuel cells, supercapacitors and lithium ion batteries. Phys Chem Chem Phys 13:15384
29. Nyholm L, Nyström G, Mihranyan A, Strømme M (2011) Toward flexible polymer and paper-based energy storage devices. Adv Mater 23:3751–3769
30. Mu ZP, Liu T, Ji X, Luo HW, Tang LJ, Cheng S (2020) A facile and cost-effective approach to fabricate flexible graphene films for aqueous available current collectors. Carbon 170:264–269
31. Bon CY, Isheunesu P, Kim S, Manasi M, Kim Y, Lee YJ, Ko JM (2018) High capacity and fast charge–discharge $Li_4Ti_5O_{12}$ nanoflakes/TiO_2 nanotubes composite anode material for lithium ion batteries. Energy Technol 6:2461–2468
32. He X, Bi T, Zheng X, Zhu W, Jiang J (2020) Nickel cobalt sulfide nanoparticles grown on titanium carbide MXenes for high-performance supercapacitor. Electrochim Acta 332:135514
33. Chen C, Yang X (2017) MnO_2 modified TiN nanotube arrays on Ti mesh for flexible supercapacitors electrode. RSC Adv 7:56440–56446
34. Cheng Q, Tang J, Ma J, Zhang H, Shinya N, Qin LC (2011) Graphene and nanostructured MnO_2 composite electrodes for supercapacitors. Carbon 49:2917–2925

35. Zhou H, Han G, Xiao Y, Chang Y, Zhai HJ (2014) Facile preparation of polypyrrole/graphene oxide nanocomposites with large areal capacitance using electrochemical codeposition for supercapacitors. J Power Sources 263:259–267
36. Dubal DP, Chodankar NR, Gund GS, Holze R, Lokhande CD, Gomez-Romero P (2015) Asymmetric supercapacitors based on hybrid CuO@Reduced graphene oxide@sponge versus reduced graphene oxide@sponge electrodes. Energy Technol 3:168–176
37. Wang S, Wu ZS, Zheng S, Zhou F, Sun C, Cheng HM, Bao X (2007) Scalable fabrication of photochemistry reduced graphene-based monolithic micro-supercapacitors with superior superior energy and power densities. ACS Nano 11:4283–4291
38. Jiang L, Ren Z, Chen S, Zhang Q, Lu X, Zhang H, Wan G (2018) Bio-derived three-dimensional hierarchical carbon–graphene–TiO_2 as electrode for supercapacitors. Sci Rep 8:1–9
39. Sahoo G, Polaki SR, Krishna NG, Kamruddin M (2019) Electrochemical capacitor performance of TiO_2 decorated vertical graphene nanosheets electrode. J Phys D Appl Phys 52:375501
40. Hossain A, Bandyopadhyay P, Guin PS, Roy S (2017) Recent developed different structural nanomaterials and their performance for supercapacitor application. Appl Mater Today 9:300–313
41. Dubal DP, Gund GS, Holze R, Lokhande CD (2013) Mild chemical strategy to grow micro-roses and micro-woolen like arranged CuO nanosheets for high performance supercapacitors. J Power Sources 242:687–698
42. Holze R (2001) In: Nalwa HS (ed) Conducting polymers. Handbook of advanced electronic and photonic materials and devices, vol. 8. Academic press, San Diego
43. Holze R, Wu YP (2014) Intrinsically conducting polymers in electrochemical energy technology: trends and progress. Electrochim Acta 122:93–107
44. Naderi HR, Mortaheb HR, Zolfaghari A (2014) Supercapacitive properties of nanostructured MnO_2/exfoliated graphite synthesized by ultrasonic vibration. J Electroanal Chem 719:98–105
45. Wu ZS, Wang DW, Ren W, Zhao J, Zhou G, Li F, Cheng HM (2010) Anchoring hydrous RuO_2 on graphene sheets for high-performance electrochemical capacitors. Adv Funct Mater 20:3595–3602
46. Zhong Y, Xia XH, Shi F, Zhan JY, Tu JP, Fan HJ (2016) Transition metal carbides and nitrides in energy storage and conversion. Adv Sci 3:1500286
47. Feng H, Wang W, Zhang M, Zhu S, Wang Q, Liu J, Chen S (2020) 2D titanium carbide-based nanocomposites for photocatalytic bacteriostatic applications. Appl Catal B Environ 266:118609
48. Cai T, Wang L, Liu Y, Zhang S, Dong W, Chen H, Yi X, Yuan J, Xia X, Liu C, Luo S (2018) Ag_3PO_4/Ti_3C_2 MXene interface materials as a Schottky catalyst with enhanced photocatalytic activities and anti-photocorrosion performance. Appl Catal B Environ 239:545–554
49. Naguib M, Come J, Dyatkin B, Presser V, Taberna PL, Simon P, Barsoum MW, Gogotsi Y (2012) MXene: a promising transition metal carbide anode for lithium-ion batteries. Electrochem Commun 16:61–64
50. Melchior SA, Raju K, Ike IS, Erasmus RM, Kabongo G, Sigalas I, Iyuke SE, Ozoemena KI (2018) High-voltage symmetric supercapacitor based on 2D titanium carbide (MXene, Ti_2CT_x)/carbon nanosphere composites in a neutral aqueous electrolyte. J Electrochem Soc 165:A501–A511
51. Lu X, Wang G, Zhai T, Yu M, Xie S, Ling Y, Liang C, Tong Y, Li Y (2012) Stabilized TiN nanowire arrays for high-performance and flexible supercapacitors. Nano Lett 12:5376–5381
52. Wang C, Lu W, Lai Q, Xu P, Zhang H, Li X (2019) A TiN nanorod array 3D hierarchical composite electrode for ultrahigh power density bromine based flow batteries. Adv Mater 31:1904690
53. Theerthagiri J, Durai G, Karuppasamy K, Arunachalam P, Elakkiya V, Kuppusami P, Maiyalagan T, Kim HS (2018) Recent advances in 2-D nanostructured metal nitrides, carbides, and phosphides electrodes for electrochemical supercapacitors: a brief review. J Ind Eng Chem 67:12–27
54. Qi H, Yick S, Francis Q, Murdock A, Van der Laan T, Ostrikov K, Bo Z, Han Z, Bendavid A (2020) Nanohybrid TiN/vertical graphene for high-performance supercapacitor applications. Energy Storage Mater 26:138–146
55. Ndiaye NM, Ngom BD, Sylla NF, Masikhwa TM, Madito MJ, Momodu D, Ntsoane T, Manyala N (2018) Three dimensional vanadium pentoxide/graphene foam composite as positive electrode for high performance asymmetric electrochemical supercapacitor. J Colloid Interface Sci 532:395–406
56. Kale SB, Lokhande AC, Pujari RB, Lokhande CD (2018) Cobalt sulfide thin films for electrocatalytic oxygen evolution reaction and supercapacitor applications. J Colloid Interface Sci 532:491–499
57. Kolathodi MS, Palei M, Natarajan TS, Singh G (2020) MnO_2 encapsulated electrospun TiO_2 nanofibers as electrodes for asymmetric supercapacitors. Nanotechnology 31:125401
58. Park S, Shin D, Yeo T, Seo B, Hwang H, Lee J, Choi W (2020) Combustion-driven synthesis route for tunable TiO_2/RuO_2 hybrid composites as high-performance electrode materials for supercapacitors. Chem Eng J 384:123269
59. Ramadoss A, Kim SJ (2013) Improved activity of a graphene–TiO_2 hybrid electrode in an electrochemical supercapacitor. Carbon 63:434–445
60. Fu W, Zhao E, Ma R, Sun Z, Yang Y, Sevilla M, Fuertes AB, Magasinski A, Yushin G (2020) Anatase TiO_2 confined in carbon nanopores for high-energy Li–ion hybrid supercapacitors operating at high rates and subzero temperatures. Adv Energy Mater 10:1902993
61. Ncube NM, Zheng H (2020) The effect of synthesis temperature on the properties of TiO_2 (B) nanorods and its precursors as anode materials for lithium-ion batteries. Mater Res Express 7:015504
62. Ramadoss A, Kim SJ (2014) Enhanced supercapacitor performance using hierarchical TiO_2 nanorod/$Co(OH)_2$ nanowall array electrodes. Electrochim Acta 136:105–111
63. Peighambardoust NS, Asl SK, Mohammadpour R, Asl SK (2018) Band-gap narrowing and electrochemical properties in *N*-doped and reduced anodic TiO_2 nanotube arrays. Electrochim Acta 270:245–255
64. Raj CC, Prasanth R (2018) Review-advent of TiO_2 nanotubes as supercapacitor electrode. J Electrochem Soc 165:E345–E358
65. Ye Y, Wang P, Sun H, Tian Z, Liu J, Liang C (2015) Structural and electrochemical evaluation of a TiO_2-graphene oxide based sandwich structure for lithium-ion battery anodes. RSC Adv 5:45038–45043
66. Han J, Hirata A, Du J, Ito Y, Fujita T, Kohara S, Ina T, Chen M (2018) Intercalation pseudocapacitance of amorphous titanium dioxide@nanoporous graphene for high-rate and large-capacity energy storage. Nano Energy 49:354–362
67. Wang Y, Song Y, Xia Y (2016) Electrochemical capacitors: mechanism, materials, systems, characterization and applications. Chem Soc Rev 45:5925–5950
68. Zhao X, Sánchez BM, Dobson PJ, Grant PS (2011) The role of nanomaterials in redox-based supercapacitors for next generation energy storage devices. Nanoscale 3:839–855
69. Noori A, El-Kady MF, Rahmanifar MS, Kaner RB, Mousavi MF (2019) Towards establishing standard performance metrics for batteries: supercapacitors and beyond. Chem Soc Rev 48:1272–1341

70. Al-zubaidi A, Asai N, Ishii Y, Kawasaki S (2020) The effect of diameter size of single-walled carbon nanotubes on their high temperature energy storage behavior in ionic-based electric double-layer capacitors. RSC Adv 10:41209–41216
71. Das S, Ghosh A (2020) Symmetric electric double-layer capacitor containing imidazolium ionic liquid-based solid polymer electrolyte: effect of TiO_2 and ZnO nanoparticles on electrochemical behavior. J Appl Polym Sci 137:48757
72. Brousse T, Crosnier O, Bélanger D, Long JW (2017) Capacitive and pseudocapacitive electrodes for electrochemical capacitors and hybrid devices. Met Oxide Supercapacitors 2017:1–24
73. Ates M, El-Kady M, Kaner RB (2018) Three-dimensional design and fabrication of reduced graphene oxide/polyaniline composite hydrogel electrodes for high-performance electrochemical supercapacitors. Nanotechnology 29:175402
74. Shi H (1996) Activated carbons and double layer capacitance. Electrochim Acta 41:1633–1639
75. Guidi G, Undeland TM, Hori Y (2008) An interface converter with reduced volt-ampere ratings for battery-supercapacitor mixed systems. IEE J Trans Ind Appl 128:418–423
76. Wu WL, Wang CW, Zhao CH, Wei D, Zhu JF, Xu YL (2020) Facile strategy of hollow polyaniline nanotubes supported on Ti_3C_2-MXene nanosheets for high-performance symmetric supercapacitors. J Colloid Interface Sci 580:601–613
77. Chen X, Jiang JJ, Yang GY, Li CB, Li YJ (2020) Bioinspired wood-like coaxial fibers based on MXene@graphene oxide with superior mechanical and electrical properties. Nanoscale 12:21325–21333
78. Guo X, Zheng S, Zhang G, Xiao X, Li X, Xu Y, Xue H, Pang H (2017) Nanostructured graphene-based materials for flexible energy storage. Energy Storage Mater 9:150–169
79. Miller EE, Hua Y, Tezel FH (2018) Materials for energy storage: review of electrode materials and methods of increasing capacitance for supercapacitors. J Energy Storage 20:30–40
80. Urgunde AB, Bahuguna G, Dhamija A, Das PP, Gupta R (2020) Ni ink-catalyzed conversion of a waste polystryrene-sugar composite to graphitic carbon for electronic double layer supercapacitors. ACS Appl Electron Mater 2:3178–3186
81. Zuo X, Zhu J, Müller-Buschbaum P, Cheng YJ (2017) Silicon based lithium-ion battery anodes: a chronicle perspective review. Nano Energy 31:113–143
82. Cho JS, Hong YJ, Kong YC (2015) Design and synthesis of bubble-nanorod structured Fe_2O_3-carbon nanofibers as advanced anode material for Li-ion batteries. ACS Nano 9:4026–4035
83. Liu Z, Kang J, Zhao Z, Zheng Y, Liu Y, Xiong C, Wang S, Yang Q (2021) Rationally designed N, P, Co-doped porous film via steam etching as self-supported binder-free anode for high-performance lithium-ion battery. Carbon 171:36–44
84. Uma BS, Sharma YC (2013) Equilibrium and kinetic studies for removal of malachite green from aqueous solution by a low cost activated carbon. J Ind Eng Chem 19:1099–1105
85. Béguin F, Kierzek K, Friebe M, Jankowska A, Machnikowski J, Jurewicz K, Frackowiak E (2006) Effect of various porous nanotextures on the reversible electrochemical sorption of hydrogen in activated carbons. Electrochim Acta 51:2161–2167
86. Bleda-Martínez MJ, Pérez JM, Linares-Solano A, Morallón E, Cazorla-Amorós D (2008) Effect of surface chemistry on electrochemical storage of hydrogen in porous carbon materials. Carbon 46:1053–1059
87. Naoi K, Simon P (2008) New materials and new confgurations for advanced electrochemical capacitors. Electrochem Soc Interface 17:34–37
88. Male U, Srinivasan P, Singu BS (2015) Incorporation of polyaniline nanofibers on graphene oxide by interfacial polymerization pathway for supercapacitor. Int Nano Lett 5:231–240
89. Burke A (2007) R&D considerations for the performance and application of electrochemical capacitors. Electrochim Acta 53:1083–1091
90. Patil DS, Teli AM, Choi WJ, Pawar SA, Shin JC, Kim HJ (2020) An all chemical route to design a hybrid battery type supercapacitor based on $ZnCo_2O_4$/CdS composite nanostructures. Curr Appl Phys 20:1416–1423
91. Zhu C, Zhai J, Wen D, Dong S (2012) Graphene oxide/polypyrrole nanocomposites: one step electrochemical doping, coating and synergistic effect for energy storage. J Mater Chem 22:6300–6306
92. Kuila T, Mishra A, Khanra P, Kim N, Lee J (2013) Recent advances in the efficient reduction of graphene oxide and its application as energy storage electrode materials. Nanoscale 5:52–71
93. Khalaj M, Sedghi A, Miankushki HN, Golkhatmi SZ (2019) Synthesis of novel graphene/Co_3O_4/polypyrrole ternary nanocomposites as electrochemically enhanced supercapacitor electrodes. Energy 188:116088
94. Wang Q, Nie YF, Chen XY, Xiao ZH, Zhang ZJ (2016) Controllable synthesis of 2D amorphous carbon and partially graphitic carbon materials: Large improvement of electrochemical performance by the redox additive of sulfanilic acid azochromotrop in KOH electrolyte. Electrochim Acta 200:247–258
95. Nquyen T, Montemor MD (2019) Metal oxide and hydroxide-based aqueous supercapacitors: from charge storage mechanisms and functional electrode engineering to need-tailored devices. Adv Sci 6:1801797
96. Ge YR, Xie X, Roscher J, Holze R, Qu QT (2020) How to measure and report the capacity of electrochemical double layers, supercapacitors, and their electrode materials. J Solid State Electrochem 24:3125–3230
97. Wang Q, Yong FN, Xiao ZH, Chen XY, Zhang ZJ (2016) Simply incorporating an efficient redox additive into KOH electrolyte for largely improving electrochemical performances. J Electroanal Chem 770:62–72
98. Tao HC, Fan Q, Ma T, Liu SZ, Gysling H, Texter J, Guo F, Sun ZY (2020) Two-dimensional materials for energy conversion and storage. Prog Mater Sci 111:100637
99. Vlad A, Singh N, Rolland J, Melinte S, Ajayan PM, Gohy JF (2015) Hybrid supercapacitor-battery materials for fast electrochemical charge storage. Sci Rep 4:4315
100. Heng I, Lai CW, Juan JC, Numan A, Iqbal J, Teo EYL (2019) Low-temperature synthesis of TIO_2 nanocrystals for high performance electrochemical supercapacitors. Ceram Int 45:4990–5000
101. Viswanathan A, Sheety AN (2017) Facile in-situ single step chemical synthesis of reduced graphene oxide–copper oxide–polyaniline nanocomposite and its electrochemical performance for supercapacitor application. Electrochim Acta 257:483–493
102. Slot TK, Yu F, Xu H, Ramos-Fernandez EV, Sepulveda-Escribano A, Sofer Z, Rothenberg G, Shiju NR (2020) Surface oxidation of $Ti_3C_2T_x$ enhances the catalytic activity of supported platinum nanoparticles in ammonia borane hydrolysis. 2D Materials 8: 015001
103. Tian Y, Yang C, Que W, He Y, Liu X, Luo Y, Yin X, Kong LB (2017) Ni foam supported quasi-core–shell structure of ultrathin Ti_3C_2 nanosheets through electrostatic layer-by-layer self-assembly as high rate-performance electrodes of supercapacitors. J Power Sources 369:78–86
104. Wang X, Fu Q, Wen J, Ma X, Zhu C, Zhang X, Qi D (2018) 3D Ti_3C_2Tx aerogels with enhanced surface area for high performance supercapacitors. Nanoscale 10:20828–20835
105. Guo M, Liu C, Zhang Z, Zhou J, Tang Y, Luo S (2018) Flexible Ti_3C_2Tx@Al electrodes with ultrahigh areal capacitance: in situ regulation of interlayer conductivity and spacing. Adv Funct Mater 28:1803196

106. Zou R, Quan H, Pan M, Zhou S, Chen D, Luo X (2018) Self-assembled MXene(Ti_3C_2Tx)/α-Fe_2O_3 nanocomposite as negative electrode material for supercapacitors. Electrochim Acta 292:31–38
107. Ambade SB, Ambade RB, Eom W, Noh SH, Kim SH, Han TH (2018) 2D Ti_3C_2 MXene/WO_3 hybrid architectures for high-rate supercapacitors. Adv Mater Interfaces 5:1801361
108. Tian Y, Yang C, Que W, Liu X, Yin X, Kong LB (2017) Flexible and free-standing 2D titanium carbide film decorated with manganese oxide nanoparticles as a high volumetric capacity electrode for supercapacitor. J Power Sources 359:332–339
109. Lu X, Zhu J, Wu W, Zhang B (2017) Hierarchical architecture of PANI@TiO_2/Ti_3C_2Tx ternary composite electrode for enhanced electrochemical performance. Electrochim Acta 228:282–289
110. Jiang H, Wang Z, Yang Q, Hanif M, Wang Z, Dong L, Dong M (2018) A novel MnO_2/$Ti_3C_2T_x$ MXene nanocomposite as high performance electrode materials for flexible supercapacitors. Electrochim Acta 290:695–703
111. Zhao MQ, Ren CE, Ling Z, Lukatskaya MR, Zhang C, Van Aken KL, Barsoum MW, Gogotsi Y (2015) Flexible MXene/carbon nanotube composite paper with high volumetric capacitance. Adv Mater 27:339–345
112. Li J, Yuan X, Lin C, Yang Y, Xu L, Du X, Xie J, Lin J, Sun J (2017) Achieving high pseudocapacitance of 2D titanium carbide (MXene) by cation intercalation and surface modification. Adv Energy Mater 7:1602725
113. Tian Y, Que W, Luo Y, Yang C, Yin X, Kong LB (2019) Surface nitrogen-modified 2D titanium carbide (MXene) with high energy density for aqueous supercapacitor applications. J Mater Chem A 7:5416–5425
114. Zhu J, Tang Y, Yang C, Wang F, Cao M (2016) Composites of TiO_2 nanoparticles deposited on Ti_3C_2 MXene nanosheets with enhanced electrochemical performance. J Electrochem Soc 163:A785–A791
115. Ghidiu M, Lukatskaya MR, Zhao MQ, Gogotsi Y, Barsoum MW (2014) Conductive two-dimensional titanium carbide 'clay' with high volumetric capacitance. Nature 516:78–81
116. Boota M, Anasori B, Voigt C, Zhao MQ, Barsoum MW, Gogotsi Y (2016) Pseudocapacitive electrodes produced by oxidant-free polymerization of pyrrole between the layers of 2D titanium carbide (MXene). Adv Mater 28:1517–1522
117. Wang F, Cao M, Qin Y, Zhu J, Wang L, Tang Y (2016) ZnO nanoparticle-decorated two-dimensional titanium carbide with enhanced supercapacitive performance. RSC Adv 6:88934–88942
118. Qu YP, Shi CJ, Cao HF, Wang YZ (2020) Synthesis of Ni-MOF/$Ti_3C_2T_x$ hybrid nanosheets via ultrasonific method for supercapacitor electrodes. Mater Letters 280:128526
119. Hu MM, Zhang H, Hu T, Fan BB, Wang XH, Li ZJ (2020) Emerging 2D MXenes for supercapacitors: status, challenges and prospects. Chem Soc Rev 49:6666–6693
120. Li YH, Deng YA, Zhang JF, Shen YY, Yang XY, Zhang WW (2020) Synthesis of restacking-free wrinkled $Ti_3C_2T_x$ monolayers by sulfonic acid group grafting and *N*-doped carbon decoration for enhanced supercapacitor performance. J Alloys Compds 842:155985
121. Nam S, Kim JN, Oh S, Kim J, Ahn CW, Oh IK (2020) $Ti_3C_2T_x$ MXene for wearable energy devices: supercapacitors and triboelectric nanogenerators. Apl Mater 8:110701
122. Zhang ZR, Yao ZP, Zhang X, Jiang ZH (2020) 2D carbide MXene under postetch low-temperature annealing for high-performance supercapacitor electrode. Electrochim Acta 359:136960
123. Weng L, Qi FY, Min YG (2020) The $Ti_3C_2T_x$ MXene coated metal mesh electrodes for stretchable supercapacitors. Mater Letters 278:128235
124. Li Y, Lu Z, Xin BJ, Liu Y, Cui YH, Hu YX (2020) All-solid state flexible supercapacitor of carbonized MXene/cotton fabric for wearable energy storage. Appl Surf Sci 528:146975
125. Hou X, Li Q, Zhang L, Yang T, Chen J, Su L (2018) Tunable preparation of chrysanthemum-like titanium nitride as flexible electrode materials for ultrafast-charging/discharging and excellent stable supercapacitors. J Power Sources 396:319–326
126. Liu M, Yang T, Chen J, Su L, Chou KC, Hou X (2017) TiN@$NiCo_2O_4$ coaxial nanowires as supercapacitor electrode materials with improved electrochemical and wide-temperature performance. J Alloys Compd 692:605–613
127. Xie Y, Wang D (2016) Supercapacitance performance of polypyrrole/titanium nitride/polyaniline coaxial nanotube hybrid. J Alloys Compd 665:323–332
128. Xie Y, Xia C, Du H, Wang W (2015) Enhanced electrochemical performance of polyaniline/carbon/titanium nitride nanowire array for flexible supercapacitor. J Power Sources 286:561–570
129. Meng Q, Cai K, Chen Y, Chen L (2017) Research progress on conducting polymer-based supercapacitor electrode materials. Nano Energy 36:268–285
130. Karthika P, Rajalakshmi N, Dhathathreyan KS (2012) Functionalized exfoliated graphene oxide as supercapacitor electrodes. Soft Nanosci Lett 02:59–66
131. Ansari SA, Khan NA, Hasan Z, Shaikh AA, Ferdousi FK, Barai HR, Lopa NS, Rahman MM (2020) Electrochemical synthesis of titanium nitride nanoparticles onto titanium foil for electrochemical supercapacitors with ultrafast charge/discharge. Sustain Energy Fuels 4:2480–2490
132. Du H, Xie Y, Xia C, Wang W, Tian F (2014) Electrochemical capacitance of polypyrrole–titanium nitride and polypyrrole–titania nanotube hybrids. New J Chem 38:1284
133. Tian F, Xie Y, Du H, Zhou Y, Xia C, Wang W (2014) Preparation and electrochemical capacitance of graphene/titanium nitride nanotube array. RSC Adv 4:41856–41863
134. Xia C, Xie Y, Wang W, Du H (2014) Fabrication and electrochemical capacitance of polyaniline/titanium nitride core–shell nanowire arrays. Synth Met 192:93–100
135. Wang T, Li K, An S, Song C, Guo X (2019) Facile and green synthesis of TiN/C as electrode materials for supercapacitors. Appl Surf Sci 470:241–249
136. Dong S, Chen X, Gu L, Zhou X, Wang H, Liu Z, Han P, Yao J, Wang L, Cui G, Chen L (2011) TiN/VN composites with core/shell structure for supercapacitors. Mater Res Bull 46:835–839
137. Anusha Thampi VV, Nithiyanantham U, Nanda Kumar AK, Martin P, Bendavid A, Subramanian B (2018) Fabrication of sputtered titanium vanadium nitride (TiVN) thin films for micro-supercapacitors. J Mater Sci Mater Electron 29:12457–12465
138. Su HL, Xiong TZ, Tan QR, Yang F, Appadurai PBS, Afuwape AA, Balogun MS, Huang YC, Guo KK (2020) Asymmetric pseudocapacitors based on interfacial engineering of vanadium nitride hybrids. Nanomaterials 10:1141
139. Sun N, Zhou D, Liu W, Shi S, Tran Z, Liu F, Li S, Wang J, Ali F (2020) Tailoring surface chemistry and morphology of titanium nitride electrode for on-chip supercapacitors. ACS Sustain Chem Eng 8:7869–7878
140. Raghavendra KVG, Vinoth R, Zeb K, Gop CWM, Sanbassivam S, Kummara MR, Obaidat IM, Kim HJ (2020) An intuitive review of supercapacitors with recent progress and novel device applications. J Energy Storage 31:101652
141. Usman M, Pan L, Asif M, Mahmood Z, Khan MA, Fu X (2016) Enhanced electrochemical supercapacitor properties with synergistic effect of polyaniline, graphene and AgxO. Appl Surf Sci 370:297–305
142. Sharavath V, Sarkar S, Ghosh S (2018) One-pot hydrothermal synthesis of TiO_2/graphene nanocomposite with simultaneous

nitrogen-doping for energy storage application. J Electroanal Chem 829:208–216
143. Liu Y, Gao T, Xiao H, Guo W, Sun B, Pei M, Zhou G (2017) One-pot synthesis of rice-like TiO_2/graphene hydrogels as advanced electrodes for supercapacitors and the resulting aerogels as high-efficiency dye adsorbents. Electrochim Acta 229:239–252
144. Tang K, Li Y, Cao H, Su C, Zhang Z, Zhang Y (2016) Amorphous-crystalline TiO_2/carbon nanofibers composite electrode by one-step electrospinning for symmetric supercapacitor. Electrochim Acta 190:678–688
145. Ates M, Bayrak Y, Yoruk O, Caliskan S (2017) Reduced graphene oxide/titanium oxide nanocomposite synthesis via microwave-assisted method and supercapacitor behaviors. J Alloys Compd 728:541–551
146. Kim TW, Park SJ (2017) Synthesis of reduced graphene oxide/thorn-like titanium dioxide nanofiber aerogels with enhanced electrochemical performance for supercapacitor. J Colloid Interface Sci 486:287–295
147. Chew SY, Ng SH, Wang JZ, Novak P, Krumeich F, Chou SL, Chen J, Liu HK (2009) Flexible free-standing carbon nanotube films for model lithium ion batteries. Carbon 47:2976–2983
148. Chou SL, Wang JZ, Choucair M, Liu HK, Stride JA, Dou SX (2010) Enhanced reversible lithium storage in a nanosize silicon / graphene composite. Electrochem Commun 12:303–306
149. Wei P, Fan M, Chen H, Yang X, Wu H, Chen J, Li T, Zeng L, Zou Y (2015) High-capacity graphene/sulfur/polyaniline ternary composite cathodes with stable cycling performance. Electrochim Acta 174:963–969
150. Zhang XY, Liu XQ, Zeng YX, Tong YX, Lu XH (2020) Oxygen defects in promoting the electrochemical performance of metal oxides for supercapacitors: Recent advances and challenges. Small Methods 4:1900823
151. Iqbal MZ, Zakar S, Tayyab M, Hider SS, Alzaid M, Afzal AM, Aftab S (2020) Scrutinizing the charge storage mechanism in SrO-based composites for asymmetric supercapacitors by diffusion-controlled process. Appl Nanosci 10:3999–4011
152. Cui J, Cao L, Zeng D, Wang X, Li W, Lin Z, Zhang P (2018) Surface characteristic effect of Ag/TiO_2 nanoarray composite structure on supercapacitor electrode properties. Scanning 2018:1–10
153. Li Z, Wang X, Wang X, Xiao T, Zhang L, Lv P, Zhao J (2018) Preparation and properties of MnO_2-TiO_2 nanotube array composite electrodes using titanium foam as the current collector. Int J Hydrogen Energy 43:8859–8867
154. Sun S, Liao X, Sun Y, Yin G, Yao Y, Huang Z, Pu X (2017) Facile synthesis of a α-MoO_3 nanoplate/TiO_2 nanotube composite for high electrochemical performance. RSC Adv 7:22983–22989
155. Xu J, Zheng F, Xi C, Yu Y, Chen L, Yang W, Hu P, Zhen Q, Bashir S (2018) Facile preparation of hierarchical vanadium pentoxide (V_2O_5)/titanium dioxide (TiO_2) heterojunction composite nano-arrays for high performance supercapacitor. J Power Sources 404:47–55
156. Mofokeng TP, Ipadeola AK, Tetana ZN, Ozoemena KI (2020) Defect engineered nanostructured Ni/MOF derived carbons for an efficient aqueous battery-type energy storage device. ACS Omega 5:20461–20472
157. Guragain D, Zequine C, Poudel T, Neupane D, Gupta RK, Mishra SR (2020) Facile synthesis of bio-templated tubular Co_3O_4 microstructure and its electrochemical performance in aqueous electrolytes. J NanoSci Nanotechnol 20:3182–3194
158. Shahen I, Ahmad KS, Zequine C, Gupta RK, Thomas A, Malik MA (2020) Organic template-assisted green synthesis of $CoMoO_4$ nanomaterials for the investigation of energy storage properties. RSC Adv 10:8115–8129
159. Deshmukh PR, Patil SV, Bulakhe RN, Pusawale SN, Shim JJ, Lokhande CD (2015) Chemical synthesis of PANI-TiO_2 composite thin film for supercapacitor application. RSC Adv 5:68939–68946
160. Muench S, Wild A, Friebe C, Haupler B, Janoschka T, Schubert US (2016) Polymer-based organic batteries. Chem Rev 116:9438–9484
161. Lian J, Wang X, Zhang W, Huang Y, Xia T, Lian Y (2016) A ternary polyaniline/active carbon/lithium iron phosphate composite as cathode material for lithium ion battery. J Nanosci Nanotechnol 16:6494–6497
162. Hui Y, Cao L, Xu Z, Huang J, Quyang H, Li J, Hu H (2017) In-situ synthesis of core-shell $Li_4Ti_5O_{12}$@polyaniline composites with enhanced rate performance for lithium-ion battery anodes. J Mater Sci Technol 33:231–238
163. Zhang Y, Sun X, Pan L, Li H, Sun Z, Sun C, Tay BK (2009) Carbon nanotube-ZnO nanocomposite electrodes for supercapacitors. Solid State Ionics 180:1525–1528
164. Wang T, Wang W, Zhu D, Huang L, Chen Y (2015) Improvement of the overall performances of $LiMn_2O_4$ via surface modification by polypyrrole. Mater Res Bull 71:91–97
165. Fedorkova A, Orinakova R, Orinak A, Talian I, Heile A, Wiemhöfer HD, Kaniansky D, Arlinghaus HF (2010) PPy doped PEG conducting polymer films synthesized on $LiFePO_4$ particles. J Power Sources 195:3907–3912
166. Xu D, Wang P, Yang R (2017) Enhanced electrochemical performance of core–shell $Li_4Ti_5O_{12}$/PTh as advanced anode for rechargeable lithium-ion batteries. Ceram Int 43:7600–7606
167. Wang X, Shen L, Li H, Wang J, Dou H, Zhang X (2014) PEDOT coated $Li_4Ti_5O_{12}$ nanorods: soft chemistry storage properties. Electrochim Acta 129:283–289
168. Cintora-Juarez D, Perez-Vicente C, Ahmad S, Tirado JL (2014) Improving the cycling performance of $LiFePO_4$ cathode material by poly(3,4-ethylenedioxythiophene) coating. RSC Adv 4:26108–26114
169. Phan TB, Luong TT, Mai TX, Mai TTT, Pham TT (2016) Effect of nano-structured graphene oxide on electrochemical activity of its composite with polyaniline titanium dioxide. Adv Nat Sci Nanosci Nanotechnol 7:015016
170. Ghosh D, Giri S, Kalra S, Das CK (2012) Synthesis and characterizations of TiO_2 coated multiwalled carbon nanotubes / graphene / polyaniline nanocomposite for supercapacitor applications. Open J Appl Sci 2:70–77
171. Palmas S, Mascia M, Vacca A, Llanos J, Mena E (2014) Analysis of photocurrent and capacitance of TiO_2 nanotube–polyaniline hybrid composites synthesized through electroreduction of an aryldiazonium salt. RSC Adv 4:23957–23965
172. Bocchetta P, Frattini D, Taglienta M, Selleri F (2020) Electrochemical development of polypyrrole nanostructures for energy applications: a review. Curr Nanosci 16:462–477
173. Boota M, Gogotsi Y (2019) MXene-conducting polymer asymmetric pseudocapacitors. Adv Energy Mater 9:1802917
174. Wang JG, Ma FC, Liang WJ, Sun MT (2017) Electrical properties and applications of graphene, hexagonal boron nitride (h-BN), and graphene/h-BN heterostructures. Mater Today Physics 2:6–34
175. Jiang L, Luo D, Zhang Q, Ma S, Wan G, Lu X, Ren Z (2019) Electrochemical performance of free-standing and flexible graphene and TiO_2 composites with different conductive polymers as electrodes for supercapacitors. Chem Eur J 25:7903–7911
176. Li Y, Zhou M, Li Y, Gong Q, Wang Y, Xia Z (2018) Structural, morphological and electrochemical properties of long-alkoxy-functionalized polythiophene and TiO_2 nanocomposites. Appl Phys A 124:855
177. Mehmood U, Ahmad SHA, Al-Ahmed A, Hakeem AS, Defalla H, Laref A (2020) Synthesis and characterization of cerium oxide impregnated titanium oxide photoanodes for efficient dye-sensitized solar cells. IEEE J Photovolt 10:1365–1370

178. Roger I, Shipman MA, Symes MD (2017) Earth-abundant catalysts for electrochemical and photo-electrochemical water splitting. Nat Rev Chem 1:0003
179. Hasan MR, Lai CW, Hamid SBA, Basirun WJ (2014) Effect of Ce doping on RGO–TiO nanocomposite for high photoelectrocatalytic behavior. Int J Photoenergy 2014:141368
180. Ren K, Liu Z, Wei T, Fan ZJ (2021) Recent developments of transition metal compounds–carbon hybrid electrodes for high energy/power supercapacitors. Nano Micro Lett 13:129
181. Larcher D, Tarascon JM (2015) Towards greener and more sustainable batteries for electrical energy storage. Nat Chem 7:19–29
182. Majumdar D, Baugh N, Bhattacharya SK (2017) Ultrasound assisted formation of reduced graphene oxide-copper (II) oxide nanocomposite for energy storage applications. Colloids Surf 512:158–170

Authors and Affiliations

Murat Ates[1] · Ozge Kuzgun[1] · Idris Candan[2]

✉ Murat Ates
mates@nku.edu.tr

[1] Department of Chemistry, Faculty of Arts and Sciences, Tekirdag Namik Kemal University, 59030 Tekirdag, Turkey

[2] Department of Physics, Kocaeli University, 41001 Izmit, Kocaeli, Turkey